

2008

Cross-Frontal Velocity and Temperature Structure of the New Jersey Midshelf Frontal Zone

Michelle Louise Aleszczyk
University of Rhode Island

Follow this and additional works at: <https://digitalcommons.uri.edu/theses>

Terms of Use

All rights reserved under copyright.

Recommended Citation

Aleszczyk, Michelle Louise, "Cross-Frontal Velocity and Temperature Structure of the New Jersey Midshelf Frontal Zone" (2008). *Open Access Master's Theses*. Paper 987.
<https://digitalcommons.uri.edu/theses/987>

This Thesis is brought to you by the University of Rhode Island. It has been accepted for inclusion in Open Access Master's Theses by an authorized administrator of DigitalCommons@URI. For more information, please contact digitalcommons-group@uri.edu. For permission to reuse copyrighted content, contact the author directly.

**CROSS-FRONTAL VELOCITY AND TEMPERATURE STRUCTURE OF THE NEW
JERSEY MIDSHELF FRONTAL ZONE**

BY

MICHELLE LOUISE ALESZCZYK

**A THESIS SUBMITTED IN PARTIAL FULFILLMENT OF THE
REQUIREMENTS FOR THE DEGREE OF
MASTER OF SCIENCE
IN
OCEANOGRAPHY**

UNIVERSITY OF RHODE ISLAND


2008

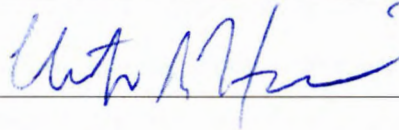
MASTER OF SCIENCE THESIS
OF
MICHELLE LOUISE ALESZCZYK

APPROVED:

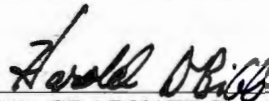
Masters Committee:

Major Professor









DEAN OF THE GRADUATE SCHOOL

UNIVERSITY OF RHODE ISLAND

2008

ABSTRACT

The cross-shelf structure of fronts, which occur during the winter months along the 30 m and 50 m isobath, are examined using remote sensing observations of the southern New Jersey shelf region. Shipboard observations show that cooler, fresher, less dense water is located inshore of the front; however, little is known of the velocity structure in the frontal zone. Surface current fields from high-frequency radar are analyzed along with surface thermal front observations to describe the cross-shelf spatial variability of surface flow with regard to the fronts. Cloud-cleared, Level 2 MODIS Thermal IR sea-surface temperature (SST) data from AQUA and TERRA from winters 2003 - 2007 are processed using an edge-detection algorithm to determine the frequency, location, strength and orientation of the fronts. The record and seasonal progressions of the temperature and velocity fields are analyzed. No evidence is found to support the Ou Tidal Diffusivity theory that predicts that front location is a function of the spring-neap cycle. Cross-shelf locations of convergence due to the surface velocity appear to increase front occurrence, which is in agreement with Hoskins' frontogenesis theory. Shear/vorticity also seems to play a role in front occurrence and front orientation. Also of note is that the location of minimum cross-shelf velocity variance is coincident with 30 m isobath fronts, while the minimum in along-shelf velocity variance is at the 50 m isobath. Furthermore, the 30 m (50 m) is the location at which the cross-shelf (along-shelf) wind-driven surface velocity component becomes greater (less) than the residual surface velocity component. Additionally, the front strength, measured by SST gradient magnitude, is inversely related to heat flux in the 50 m isobath region and nearly unrelated to the heat flux in the 30 m isobath region.

ACKNOWLEDGEMENTS

Much appreciation is due to my advisor, David Ullman, for his utmost patience and constant guidance. Additional thanks are extended to Chris Kincaid, Scott Rutherford, and Josh Kohut. Fellow students Justin Rogers and Lauren Decker have been integral to the completion of this thesis. Last but not least, I'd like to thank my parents for their continual support and faith.

This research was made possible by the National Science Foundation Grant *OCE-0550770: Observations of the Structure and Dynamics of Midshelf Fronts*.

TABLE OF CONTENTS

Abstract	ii
Acknowledgements	iii
Table of Contents	iv
List of Figures	v
Cross-Frontal Velocity and Temperature Structure in the New Jersey Midshelf	
Frontal Zone	1
1 Introduction	1
1.1 Background Definitions and Equations	1
1.2 Front Theories	2
1.3 Importance of Fronts	3
1.4 Previous Related Work	4
2 Data and Methodology	6
2.1 Study Area and Analysis Period	6
2.2 Sea Surface Temperature Fronts	7
2.3 Surface Velocities	8
2.4 Buoy Data	9
2.5 Tidal Amplitude	10
3 Results	11
3.1 Sea Surface Temperature	11
3.2 Surface Velocities	15
3.3 Comparisons	20
4 Discussion and Conclusions	23
4.1 Ongoing Research	25
Bibliography	62

LIST OF FIGURES

1	Geographic Location of Various Types of Fronts that occur on the New Jersey Shelf	26
2	Midshelf Front Hydrography	27
3	Previous Detection of Fronts in Middle Atlantic Bight	28
4	Shelf region of southern New Jersey	29
5	Sea Surface Temperature Image Processing	30
6	Annual Variation in Winter Front Probability	31
7	Monthly Variation in Front Probability	32
8	Annual Variation in Front Cross-shelf Location on Line B	33
9	Monthly Variation in Front Cross-shelf Location on Line B	34
10	Cross-shelf Bathymetry of Line B	35
11	Daily Variation in Front Cross-shelf Location	36
12	Lomb Periodogram of Front Cross-shelf Location	37
13	Annual Variation in SST Gradient Magnitude	38
14	Monthly Variation in SST Gradient Magnitude	39
15	Annual Variation in SST Gradient Direction	40
16	Monthly Variation in SST Gradient Direction	41
17	Winter Mean Current Velocity	42
18	Upshef Incident	43
19	Winter Spatial Mean Current Components	44
20	Velocity Variance as a function of Distance Offshore	45
21	Monthly Spatial Mean Current Components	46
22	Shelf-wide Current Direction Variations	47
23	Temporal Variability of Cross-shelf Velocity along Line B	48
24	Temporal Variability of Along-shelf Velocity along Line B	49

25	Temporal Variability of Mean Current Components along Line B	50
26	Temporal Variability of Line B Cross-shelf Velocity Anomaly	51
27	Temporal Variability of Line B Along-shelf Velocity Anomaly	52
28	Correlation between Wind and Current as a function of Offshore Distance . . .	53
29	Transient, Wind-driven, and Residual Velocity Variance with Line B Distance Offshore	54
30	Annual Variation of Wind Direction Distribution	55
31	Divergence and Front Probability as a function of Distance Offshore	56
32	Composite Analysis of January 28 - March 18 2003	57
33	Composite Analysis of December 1 - December 31 2005	58
34	Composite Analysis of February 1 - February 28 2007	59
35	Winter and Monthly Variation of Heat Flux	60
36	Heat Flux versus SST Gradient Magnitude	61

Cross-Frontal Velocity and Temperature Structure in the New Jersey Midshelf Frontal Zone

1 Introduction

This work is part of a National Science Foundation research grant (*OCE-0550770: Observations of the Structure and Dynamics of Midshelf Fronts*) to study the midshelf front (MSF) along the continental shelf of southern New Jersey. The focus of the grant work is to characterize the vertical structure of these fronts. The focus of this work is the analysis of the surface structure/ frontal signature using remote sensing.

1.1 Background Definitions and Equations

Fronts exist throughout the ocean and range in length from 1 to 1000 km (*Federov, 1986*). They can mark the boundary between two water masses and are identifiable by large horizontal gradients in physical, chemical, and/or biological properties. There are a variety of frontal types which have distinct locations, vertical signatures, durations, intensities, and formation mechanisms.

Prominent frontogenesis mechanisms are tidal friction, river discharge, convergence, and/or wind. The most common types are tidal mixing fronts (TMF), buoyant outflow fronts (BOF), shelf break fronts (SBF), and MSFs. A schematic of where these fronts manifest on the New Jersey continental shelf is displayed in figure 1. Tidal mixing fronts form between stratified and unstratified regions. They develop as a result of solar heating dominating the stratified region and vertical mixing dominating in the unstratified region (*Hill and Simpson, 1989*). Buoyant outflow fronts arise as a result of significant freshwater discharge from coastal estuaries (*Yankovsky and Chapman, 1997*). In the case of the New Jersey MSF, the Hudson River outflow is considered to be a surface-advected BOF (*Ou et al., 2003*). However, *Narayanan and Garvine (2002)* found that a surface-advected BOF can become a bottom-advected BOF at large distances from the

source. The isopycnals of a BOF are nearly vertical, sloping from the bottom to the surface (figure 2). Shelf break fronts have a similar vertical structure and mark the barrier between cool, fresh inshore waters and warm, salty slope waters. They occur year-round offshore of the 200 m isobath and have an associated geostrophic jet. This jet is approximately 10 to 25 km wide and flows southwestward at 20 to 50 cm/s according to *Fratantoni et al.* (2001) and *Oey* (1986). Furthermore, the cross-front velocities are on the order of 1 cm/s while along-front velocities are one order of magnitude larger ($O(10)$ cm/s) (*Oey*, 1986).

Midshelf fronts have been observed in the shelf seas around the British Isles (*Robinson*, 1985), the Gulf of Mexico (*Huh et al.*, 1978), the East China Sea (*Hickox et al.*, 2000) (*Chang et al.*, 2006), the South Atlantic Bight (*Oey*, 1986), and the Mid-Atlantic Bight (MAB) (*Ullman and Cornillon*, 2001). The MSF on the New Jersey coastline is a wintertime (January - March) feature that separates cooler, fresher, less dense inshore water from warmer, saltier outer shelf water and tends to be aligned with the local bathymetry (*Ullman and Cornillon*, 2001). Also, since it appears only in the winter, the significant decrease of solar heating and weak stratification of the offshore waters suggests that this feature is not a tidal mixing front. Cross-shelf hydrographic sections (figure 2) show how the cross-shelf structure is similar to a type 1 front as defined by (*Hill and Simpson*, 1989), in which isopycnals extend from the bottom to the surface in the frontal zone.

Like the SBF, the MSF is believed to have an associated geostrophic velocity jet. This jet would be smaller in magnitude, due to weaker density gradients in the midshelf region. The magnitude of such a jet is estimated using the thermal wind equation (equation 1).

$$\frac{\partial v_g}{\partial z} = \frac{-g}{f\rho_o} \frac{\partial \rho}{\partial x} \quad (1)$$

So as density (ρ) varies in the cross-shelf (x) direction, the along-shelf geostrophic velocity (v_g) varies in the vertical (z). The other variables are the coriolis parameter (f), average density (ρ_o), and gravity (g). Using the winter 2007 research cruise data and assuming $v_g = 0$ at the bottom, I calculated an approximate value of -5.71 cm/s for the v_g ($g = 9.8$ m/s, $f = 0.92 \cdot 10^{-4}$ s $^{-1}$, $\rho_o = 1026.48$ kg/m 3 , $\partial \rho = 0.11$ kg/m 3 , $\partial x = 10$ km, $\partial z = 50$ m).

1.2 Front Theories

A major hypothesis of MSF forcing mechanism is the Tidal Diffusivity (TD) theory described by *Ou et al.* (2003). While this theory attempts to explain why fronts form, there is another theory to note by *Hoskins* (1982), which discusses how an existing front can be affected.

Of particular interest to this work is how *Hoskins* (1982) describes the temporal variation of a horizontal gradient as a function of the velocity gradient field. It has been shown that fronts occur along isobaths, therefore my concern is primarily with the cross-shelf temperature gradient, $\partial T / \partial x$.

$$\frac{d}{dt} \left(\frac{\partial T}{\partial x} \right) = -\frac{\partial u}{\partial x} \frac{\partial T}{\partial x} - \frac{\partial v}{\partial x} \frac{\partial T}{\partial y} + \frac{1}{h} \frac{\partial F}{\partial x} + \frac{\partial S}{\partial x} \quad (2)$$

In this equation, u and v are horizontal velocities in the x (cross-shelf) and y (along-shelf) directions. F is the turbulent heat flux at the sea surface and S is the source term of radiative heating. For the purposes of this analysis, I will concentrate on the first two terms on the right hand side (RHS). The first term on the RHS is a measure of convergence by the horizontal velocity field upon a temperature gradient. If convergence (divergence) occurs, this term tends to strengthen (weaken) the total cross-shelf temperature gradient (on the LHS). And the second term on the RHS quantifies the effects of shear flow in the horizontal velocity upon a temperature gradient. Assuming $\partial T / \partial y < 0$, when positive (negative) shear occurs, this term tends to strengthen (weaken) the total cross-shelf temperature gradient (on the LHS).

Ou's analytical model assumes a dominance of cross-shelf tidal motion. He assumes that buoyancy flux, F_x , is constant across the shelf and equal to its value at the coast. He argues that $F_x = h \langle k \rangle \rho_x$, such that $\langle k \rangle$ is tidal diffusivity, h is depth, $h \langle k \rangle$ is total (vertically-integrated) diffusivity, and ρ_x is the cross-shelf density gradient. Furthermore, *Ou et al.* (2003) assert that there is a total diffusivity minimum and consequently a density gradient maximum at midshelf. Most importantly, frontal depth is predicted to have a square-root dependence on tidal amplitude (*Ou et al.*, 2003). They assert that a front should migrate inshore/offshore with the spring-neap tidal cycles (of 14 and 28 days). Also, In this case, the existence of a front has no effect on the rate of cross-shelf exchange of properties.

1.3 Importance of Fronts

If the MSF is a smaller version of the SBF, then there may be enriched biological activity in the vicinity of MSFs due to vertical advection of nutrients. For instance, on the Argentinean coast, a band of high phytoplankton concentration, due to nutrient upwelling, appears along the SBF (Romero *et al.*, 2006). Also, large quantities of fish, scallops, and zooplankton are found along this SBF region (Brunetti *et al.*, 1998). Another example of the influence of fronts on primary production is off the coast of California. Albacore tuna are located on the warm, offshore of an upwelling front, while salmon are on the colder, inshore side (Breaker *et al.*, 2005).

Additionally, fronts can act as a barrier to cross-shelf exchange of chemical and geological constituents, and this cross-shelf variation can be traced via water mass characteristics (Blanton, 1986).

1.4 Previous Related Work

Fronts

The along-shelf coastal current in the MAB is influenced by the bathymetry, since the inner shelf is quite shallow and gently sloping (Whitney and Garvine, 2005). Ullman and Cornillon (2001) found that winter (January-March) MSFs along the northeastern U.S. coast predominantly occur in the vicinity of the 50 m isobath (figure 3), where bottom depth on the shelf changes most rapidly. A second region further inshore in the vicinity of the 30 m isobath, and with slightly lower frontal probabilities, is also noted by Ullman and Cornillon (2001). The 50 m isobath MSF appears to be approximately 5 km wide (Ullman and Cornillon, 2001). This MSF was first noted in Ullman and Cornillon (1999), in which they used an edge-detection algorithm to perform a 12 year (1985 - 1996) time series analysis of sea surface temperature (SST) images to obtain frontal length, width, depth, and other coordinating information. The surface signature of these midshelf SST fronts appear and disappear on a regular basis throughout the winter and take approximately 3 to 5 weeks to form or decay (Ullman and Cornillon, 2001).

Not only have 50 m isobath fronts been found along the eastern U.S. coast, but they have

also been observed along the eastern coast of China. *Hickox et al.* (2000) found seasonally persistent cold surface thermal fronts that align along the 50 m isobath in the East China Sea (ECS). Just south of the ECS, in the Taiwan Strait, wintertime (December - February) 50 m fronts were detected (*Chang et al.*, 2006). They noted a widening and shoreward movement of the frontal band over the winter period.

The relationship between wind and SST front dynamics was another aspect of the work done by *Ullman and Cornillon* (2001). They concluded that offshore winds result in stronger fronts, and vice versa with regard to onshore winds. Also, offshore winds during the months of January to March are typically caused by Cold Air Outbreaks (CAO) and tend to induce rapid surface cooling, especially over the shallower, well-mixed waters (*Ullman and Cornillon*, 2001). *Csanady* (1978) found that a coastal front is strengthened by down-shelf winds and is weakened by up-shelf winds.

Surface Circulation and Wind Influence

The high-frequency (HF), Coastal Ocean Dynamics Application Radar (CODAR) manufactured by CODAR Ocean Sensors has been used extensively along the MAB, particularly in the Block Island and the New Jersey shelf region. This equipment enables constant observation of coastal flow with high temporal resolution (hourly) and wide spatial coverage. The velocity vectors have a 6 km resolution out to approximately 200 km from the coast.

According to *Beardsley et al.* (1976), the MAB sub-tidal shelf currents are predominately wind-driven. Furthermore, winds in this region are most frequently from the W and NW (*Saunders*, 1977) and vary on time scales of $O(2 - 10)$ days (*Mooers et al.*, 1976). But currents not only are influenced by winds, but are also large scale free-waves from the far field that migrate along the coast and affect the current in this region (*Ou et al.*, 1981).

This area off the coast of New Jersey is very well-sampled. *Kohut et al.* (2004) noted two dominant regimes of hydrographic variability, which are summer stratified and winter mixed. They found that in the winter, the current response is less correlated with the wind and there is an influence of bottom topography on current variability. LaTTE (Lagrangian Transport and

Transformation Experiment) was conducted during the spring of 2005, from which *Gong et al.* (2006) discovered five major current pathways visible in the NJ shelf, which tended to flow along the SBF, the MSF, and inner shelf. Additionally, they concluded that the pathways were strongly wind driven and influenced by bottom topography. Surface currents, sea level and winds from August 2002 - January 2004 in this region were analyzed by *Dzwonkowski et al.* (2008a). They suggested that shelf wide cross-shelf surface flow is driven by cross-shelf winds. Further analysis of this data via an EOF analysis of the sub-inertial surface velocity structure identified flow patterns (*Dzwonkowski et al.*, 2008b). They found shelf wide and point flow impact offshore transport. Also, *Castelao et al.* (2008) analyzed data from satellites, gliders, buoys, and the HF radar during the summer/spring of 2006 and found an offshore jet south of the Hudson shelf valley that was correlated to upwelling winds. These are just a glimpse of the abundant research conducted in this region.

2 Data and Methodology

2.1 Study Area and Analysis Period

The analysis region is the shelf off southern New Jersey in the MAB (figure 4). These waters were selected due to the continuous monitoring program carried out by Rutgers University's Coastal Ocean Observation Lab (COOL). This includes a five year record of surface currents measured via HF radar. Another reason for selection is that this region was found to exhibit a strong MSF signal in winter (*Ullman and Cornillon, 1999*). The general orientation of the coastline in this area is 38°T , defined as θ_{coast} . Preliminary analysis of SST imagery found that fronts were present along the 50 m isobath and, almost as frequently, along the 30 m isobath. In order to separately describe the fronts in the vicinity of each of these isobaths, two 30 km (cross-shelf width) by 100 km (along-shelf length) boxes were drawn (one around the 30 m isobath and one around the 50 m isobath). These boxes, referred to as Box 30 and Box 50, are shown in figure 4. Three cross-shelf transect lines denote the locations along which the HF radar derived surface velocities were obtained. From north to south, each line is separated by 50 km (in the along-shelf direction) and are labeled as line A, line B, and line C. Each transect originates approximately 30 km from the shoreline and has a length of 120 km.

Ullman and Cornillon (1999) found that fronts along the shelf were common during January - March. Preliminary analysis of SST imagery showed that front occurrence increased in December and decreased in March. In order to analyze the frontogenesis (front generation) and frontolysis (front dissipation), the winter period was defined to be from 0000 01 December through 2359 31 March. All data and coordinating variables are in Universal Time (UTC), also known as Greenwich Mean Time (GMT). The year number of a given winter will be defined as the year within which that winter ends. For instance, the winter of 2003 includes December 2002, January 2003, February 2003, and March 2003. Data from five winters (2003 - 2007) are used.

Further mention of a record mean will be with regard to these years. The winter mean consists of data within the four months of that winter. The monthly mean consists of the average

of values found during the days within that month. And the daily mean will be defined as the average of the given property from 0000 to 2359 of that day.

2.2 Sea Surface Temperature Fronts

Sea surface temperature (SST) imagery was obtained from NASA's Ocean Color Web (<http://oceancolor.gsfc.nasa.gov/>). Level 2, Thermal Infrared, 11 μm , day and night SST from Moderate Resolution Imaging Spectroradiometer (MODIS) aboard AQUA and TERRA satellites were downloaded. These polar-orbiting satellites each capture 2 to 4 images of the MAB per day, resulting in approximately 725 images over the course of a winter (01 December to 31 March). The swaths obtained had latitudinal bounds of 38°N to 42°N, a longitudinal bounds of 74°W and 68°W and a resolution of 1 km.

The processing of SST data began with converting the files from hdf to netCDF. This is the format required by the histogram based edge-detection algorithm, which is explained in the next paragraph. Images were cloud cleared using the inherent MODIS quality assurance variable known as quality flag. For each SST pixel within each image, there is a coordinating quality flag value ranging from 0 to 3. The most liberal quality flag value of 3 was used to mask the SST values at which there were clouds and swath edge errors. Examples of raw and cloud masked images are shown in figure 5.

After cloud-masking, each SST image was processed by the edge-detection algorithm (EDA) developed by *Cayula and Cornillon* (1995) to objectively detect fronts. This EDA was first developed by *Cayula and Cornillon* (1992) to detect surface thermal fronts in single AVHRR images and was later improved upon to include multi-image processing using a five day sliding temporal window and a 32 by 32 pixel sliding window (*Cayula and Cornillon*, 1995).

The EDA outputs two ascii files of front pixel locations, one with latitude and longitude, the other with pixel coordinates, for every input SST image. Figure 5b is an example cloud-masked SST image with fronts overlaid. Front locations, along with bathymetry data and the original SST images were used to make a front database. The database includes a range of information about each front pixel: satellite passage time, latitude, longitude, water depth, depth gradient

magnitude, depth gradient direction, SST gradient magnitude, and SST gradient direction.

Given that this shelf region is cloud-free only 15% to 30% of the time over the months of my analysis, it is necessary to take into account the fact that a pixel cannot be detected as a front if the pixel is cloud covered. This is done using a quantity called percent front probability. Percent front probability over a given time period is calculated as the number of times a given pixel is identified as a front divided by the number of times that same pixel is identified as clear, in other words has a valid SST value.

The cross-shelf temperature structure in this region is such that warm waters are generally found offshore of cold waters. Consequently, the analysis of front location and SST gradient magnitude will be limited to front pixels that meet this criterion, which have been referred to as cold fronts (*Ullman and Cornillon, 1999*).

From the database information, a variety of variables were calculated and analyzed to describe the temporal variation in location and strength of the cold fronts. Using the front pixel latitudes and longitudes, the intersection location of line B and front segments within Box 30 (figure 4) are averaged to make daily, monthly, yearly and record mean front cross-shelf locations. While for SST gradient magnitude and SST gradient direction all front pixels within Box 30 were averaged into daily, monthly, yearly and record mean values. A similar methodology was used for Box 50.

2.3 Surface Velocities

Rutgers University maintains a HF radar array off the coast of New Jersey. The coverage array extends from Long Island to a few nautical miles past Delaware Bay, and from a few kilometers offshore out to the shelf break. The 4.55 MHz, long-range HF radar characterizes the top 2.4 m of surface flow with 3 hour averages. There are four stations in New Jersey from which radials were collected. From north to south, they are Sandy Hook, Loveladies, Tuckerton, and Wildwood (figure 4). The Tuckerton site is believed to have produced erroneous radials (*Donglai Gong, personal communication*). Data from this site were not included in computing current vectors. From 2002 through 2004 these radials are output at 3 hour increments, whereas

from 2005 to 2007 they are output on hourly intervals.

Current vectors were estimated along each of the three cross-shelf lines every 5 km using the least squares method of *Lipa and Barrick (1986)*, using an averaging radius of 10 km. Points with >10% temporal coverage and ≤ 1.25 map error are used. Missing data were linearly interpolated. Each component, u_{codar} (East) and v_{codar} (North) was low-pass filtered using a 4th order, 36-hour cutoff period, Butterworth filter. The velocity vector (resultant of u_{codar} and v_{codar}) was resolved into cross-shelf (u), positive offshore, and along-shelf (v), positive up-shelf components towards θ_{coast} (equations 3 and 4).

$$u = u_{codar} * \cos(\theta_{coast} * \pi/180) + v_{codar} * \sin(\theta_{coast} * \pi/180) \quad (3)$$

$$v = -u_{codar} * \sin(\theta_{coast} * \pi/180) + v_{codar} * \cos(\theta_{coast} * \pi/180) \quad (4)$$

The cross-shelf divergence and shear, defined as $\partial u/\partial x$ and $\partial v/\partial x$, were calculated from u , v and the distance between points.

The spatial mean current is defined as the average current vector calculated from all 75 points (on all three lines). Due to reliability and consistency of surface velocity vectors, a portion of the analysis will be limited to line B. There are several lengthy temporal gaps in these data, which are due to one or more of the CODAR sites having no radials. Due to the geometric positioning of the sites, it is frequently the case that the inshore 4 to 5 km portion of line C does not have data.

2.4 Buoy Data

In this study region, there are two buoys operated by the National Data Buoy Center (NDBC). The more northerly one is located south of Long Island (44025) and the other is off Delaware Bay (44009) (figure 4). The water depths at these locations are 36.3 m and 28 m respectively. Historical meteorological data for each buoy were downloaded from the NDBC website (<http://www.ndbc.noaa.gov/>). From these files, air temperature ($^{\circ}\text{C}$), surface water temperature ($^{\circ}\text{C}$), dewpoint temperature ($^{\circ}\text{C}$), surface atmospheric pressure (mb), wind speed (m/s), and wind direction (in degrees clockwise from True North) were extracted.

It is assumed that winds are spatially uniform over the region of interest and are calculated accordingly. First winds were converted from meteorological convention, where wind direction is defined as the direction from which the wind is blowing, to the oceanographic convention, where wind direction is defined as towards which the wind is blowing. The wind speed and direction were converted into u_{wind} and v_{wind} components, with $90^\circ T$ as the positive x-direction. Each of the components from each buoy were low-pass filtered using the same filter as the surface velocities. The u_{wind} from buoy 44009 and u_{wind} from buoy 44025 were averaged. This was also done with v_{wind} to obtain a single hourly wind vector for the entire region. The resultant hourly wind vector (made by u_{wind} and v_{wind}) was resolved into cross-shelf and along-shelf components just as surface velocity had been in equations (3) and (4).

The sensible heat flux (W/m^2) and latent heat flux (W/m^2) were calculated using the Air-Sea MatLAB Toolbox (http://ecco2.jpl.nasa.gov/data1/matlab/air_sea/) using the buoy variables: wind speed, air temperature, dew point temperature, and air pressure. The Air-Sea toolbox calculations are based on *Fairall et al. (1996)*'s formulations for surface fluxes. Fluxes from the ocean to the atmosphere, which dominate during the winter, are marked by negative values. Further references to heat flux are the sum of sensible and latent heat fluxes.

2.5 Tidal Amplitude

Sea level data were obtained from Atlantic City, NJ (figure 4), Station ID 8534720, from NOAA's website (<http://www.co-ops.nos.noaa.gov/>). Historic, verified, hourly water levels in meters with a MLLW datum were downloaded. They were then complex demodulated at the M_2 tidal frequency to get the tidal amplitude (m). Complex demodulation uses a least squares algorithm to determine the amplitude change at a specific frequency over the course of a particular time series.

3 Results

3.1 Sea Surface Temperature

In this section, I will describe the temporal variability of fronts using averaged statistics. The four variables, which are derived solely from the SST images, are percent front probability, front location, SST gradient magnitude, and SST gradient direction. They will be described in terms of their record, annual, and monthly variability.

Front Probability

Examination of front probability maps (figure 6) shows that there is significant variability in position, width, and occurrence of frontal zones over the five winters. The record mean percent probability (figure 6f) shows that along the 30 m isobath, the highest percent probabilities occur directly on that isobath, whereas, for the 50 m isobath, the highest probabilities occur 5 km to 10 km offshore of that isobath. It is important to note that high front probabilities are not observed in the vicinity of the SBF (offshore of the 200 m isobath) due to the method of cloud-clearing used. By using a mask value of 3, pixels with strong temperature gradients, on the order of $1^{\circ}\text{C}/\text{km}$, are masked. I verified that this was not occurring in the middle and inner shelf, since SST gradients are smaller in magnitude than the SBF. Just south of 39°N there is a bend in the 50 m isobath. South of this location, the magnitude of front percent probability of fronts along the 50 m isobath decreases while the width of the frontal band increases. Similarly, south of 39.3°N there is a bend in the 30 m isobath, south of which the frontal band widens and front probability decreases. Also note that the 30 m isobath appears to have an additional, less frequent band about 20 km inshore of it. This feature is more apparent in front probability for each winter (figure 6a-e), and is the next focus of my analysis.

In the record mean front probability map, fronts are on both the 30 m and 50 m isobath, however, the front probability images for each of the five winters show that this is not the case during every year. In 2003, fronts are well defined on the 30 m and 50 m isobath south of the bend in each respective isobath. North of these points, there appears to be an increased number

of fronts in between these isobaths. In 2004 the frontal bands are most distinguishable along the 30 m and 50 m isobaths north of their bends. South of that point, the 50 m isobath frontal band appears to be oriented north-south until it reaches the 200 m isobath. The most anomalous year for front probability is 2005, during which there appear to be few fronts along the 50 m isobath. And in 2006, there appears to be a less frequent front along the 30 m isobath. Also during this year, the 50 m frontal band is its widest and most consistently along the entire 50 m isobath. In 2007, the 30 m isobath front is more frequent south and inshore of its bend. The 50 m isobath during this year is most coherent from the Hudson Canyon to its bend, south of which frontal bands are more patchy and displaced offshore.

A goal is to find out when these fronts develop or dissipate over the winter months. A five year record monthly average of percent front probability was calculated for each of the four calendar months (figure 7). In December, there is a more narrow region of high probability, which for the 50 m isobath is positioned north of the bend. In January, the high probability frontal band widens, and along the 50 m isobath it disconnects just north of the bend. In February, the 30 m isobath frontal band has its highest percent probability, particularly on and inshore of the isobath. Also, the 50 m frontal band is almost twice as wide as it was during January. This is due to high variability over that month of each given year, rather than the variability between years. This was confirmed by examining the individual monthly percent front probabilities (not shown). In March, the front probabilities decrease and the frontal bands narrow. Note that between 39.2°N and 39.3°N there is a high probability of fronts in between the 30 m and 50 m isobaths.

Front Location

In attempts to more accurately quantify the cross-shelf movement of each frontal band, the mean front location was calculated for each day, month, and winter. From this I am able to see that, in Box 30, fronts have a seasonal perturbation of less than +5 km offshore of the isobath and have a record mean front location of 47 km offshore (figure 8). On the other hand, fronts in Box 50 have a seasonal perturbation of less than +10 km offshore of the isobath and a record mean

of 98 km offshore. It is important to note that in 2005, the 30 isobath front was farthest offshore during that year, while the 50 m isobath front is farthest inshore during that year. However, this value is biased given that there are no fronts observed in Box 50 along line B during the month of February, which is the month with the greatest offshore distance over the record (figure 9b).

In the front probability plots, there appears to be no consistent pattern of front location for a specific calendar month (figure 7). Also, the record mean change in distance offshore over the winter season is less than 5 km (figure 9). Note that between February 2004 and March 2004 that the front location in Box 30 increases by almost 12 km. From the front probability (not shown) this is not the 50 m front moving inshore. Coincidentally, there is a dramatic decrease in percent front probability and frontal band width in Box 50 during this month as well. March is also noteworthy due to the fact that in Box 50 (figure 9b) between February and March, every year, the monthly mean decreases by 5 km.

In the study area, the water depth generally increases with distance offshore (figure 10). The Ou theory argues that front location (depth) will be a function of tidal amplitude and this should vary over the spring-neap cycle (14 and 28 day periods). Time series of daily mean front location (figure 11) do not exhibit visual periodicity, but the gapiness of the data does not allow definitive conclusions to be drawn. For this reason, a spectral analysis was performed. The spectral analysis of the daily mean front location over the entire record was performed using the Lomb method (*Press et al.*, 1992). The lomb normalized periodogram is ideal for time series with long gaps. The benefit of using this over a fast fourier transform (FFT), is that the FFT spectrum of an interpolated time series can result in false low-frequency bands of high power. Given the uneven temporal spacing and long gaps between seasons, the Lomb method was used.

In Box 30 the only spectral estimate greater than the significance level is at 90 days, which is the seasonal/winter cycle (figure 12a). Although there are bands of increased significance near the 14 days and 28 days, there is not conclusive evidence of spring-neap frontal movement that would support Ou's theory. Correlation coefficients were calculated for the 30 m front location and tidal amplitude, the 50 m front location and tidal amplitude, and the 30 m front location and the 50 m front location. They are 0.06, -0.07, and -0.08 respectively, which are not significantly

different from zero. Thus, the front location time series do not indicate significant movement over the spring-neap cycle.

Sea Surface Temperature Gradient Magnitude

The SST gradient magnitude is used as a measure of front strength. The annual mean SST gradient magnitude of front pixels in Box 30 seems to vary inversely with mean gradient magnitude in Box 50 (figure 13). Over the five year period, SST gradient magnitude in Box 30 is larger than those in Box 50 every year except 2007. The likely causes of this anomaly are discussed in later sections. Also of note is the large difference between SST gradient magnitudes in each box during 2005. The small magnitude in Box 50 is due to below average magnitudes during February 2005 and March 2005 (figure 14), which are also the months where there are decreased front probabilities in that region. The variability of the record monthly mean is greatest in Box 50. The record mean gradient magnitude decreases between December and March in Box 50, while in Box 30 it increases over this period. Note the minimum in Box 30 in January 2007, which is believed to be due to warmer than average December and January during that winter (visible in the monthly mean SST, not shown).

Sea Surface Temperature Gradient Direction

The gradient direction is defined as the direction towards warmer water. The winter mean SST gradient direction ranges between 99°T and 110°T (figure 15), which are in agreement with the values found by *Ullman and Cornillon (2001)*. Given that the cross-shelf direction is 128°T ($\theta_{\text{coast}}+90^\circ$), this means the gradient direction is slightly upshelf, such that $\frac{\partial T}{\partial y} > 0$. Therefore in order for $\frac{\partial T}{\partial x}$ to increase (decrease), the shear at that cross-shelf location must be negative (positive). Also, SST gradient direction in Box 30 is typically more in the along-shelf direction than the SST gradient direction in Box 50, every year except for 2005.

Over the winter months, there is not much greater than a 10° change in orientation (figure 16), except for in Box 50 during February 2005 and March 2004. The February 2005 direction is likely extremely biased given that there are only 20 front segments in that month, while during

other months number of front segments are $O(100)$ per month. In March of 2004, there is a significant decrease in the number of front segments, by far the largest decrease of any month (down by 500 segments from February 2004).

3.2 Surface Velocities

This section describes how the current components, cross-shelf and along-shelf velocity, vary in magnitude, direction, and their gradient magnitudes vary with distance offshore (along the 3 cross-shelf lines) over the winter months of the record. The majority of the analysis focuses on the cross-shelf and along-shelf surface velocities individually, and towards the latter part of this section just line B is discussed. The relationship between wind and surface current, particularly the variation of wind influence with distance offshore is also described.

Annual Variations Surface Velocity

The winter record mean surface flow is predominately downshelf and offshore, and there is significant cross-shelf variation in current magnitude and direction (figure 17). Lines B and C are most similar over the entire record. The current magnitude typically increases offshore of the 50 m isobath. In 2003, 2004, and 2005, there is little cross-shelf variability in current direction, particularly offshore of the 30 m isobath. Data from 2006 and 2007 show the current inshore of 50 m and along lines B and C is strongly aligned with or to the left of the wind.

It may seem as though there is a jet in the winter mean velocity vectors during 2007 (figure 17e). There is anomalous event, hereafter referenced as "Upshelf Incident," during this winter from February 2nd - 18th (figure 18c). With the velocities during this time period taken out (figure 18d), the 2007 winter mean velocity field appears to be more similar to the 2006 winter mean velocity field (figure 17d). Along lines A and B there does appear to be a 30 km wide band, offshore of the 50 m isobath, of increased current velocity.

The record spatial mean cross-shelf velocity is 4.12 cm/s while the record spatial mean along-shelf velocity is -4.37 cm/s (figure 19). The standard deviations of each are 1.67 cm/s and 2.90 cm/s, respectively. The strongest cross-shelf velocities are in 2006 and 2007 and the

weakest in 2003 and 2005.

There is much more variation in the along-shelf velocities, which typically range from -40 cm/s to 40 cm/s. Cross-shelf velocities generally range between -20 cm/s and 20 cm/s. The strongest negative along-shelf velocity is in 2005 and the weakest is in 2007. Another measure of temporal velocity variability is velocity variance. Variance is a measure of energy in the current fluctuations over all timescales. For each point along line B, variance of the low-passed u and v for each given winter was calculated and the results are plotted versus offshore distance (figure 20). A notable finding is that for both velocity components, there tends to be a midshelf location of minimum variance. For cross-shelf velocity variance (figure 20a), the minimum is located 45 km offshore (at the 30 m isobath). And, for along-shelf velocity variance (figure 20b), the minimum is located 90 km offshore (at the 50 m isobath). Also, important to note is that the velocity variance in the along-shelf direction is typically 3 to 4 times greater than the cross-shelf direction.

Monthly Variations in Surface Velocity

The record monthly spatial mean (averaged over all times and all locations) cross-shelf velocity decreases by approximately 1 cm/s each month of the winter (figure 21). A noteworthy feature in the individual years is a 7 cm/s difference between cross-shelf velocity during February 2005 and February 2006. The highest magnitude in along-shelf velocity occurs during January 2005, which is -11.7 cm/s. The along-shelf winter mean for 2005 is heavily influenced by the January 2005 along-shelf velocity, given that it is nearly three times the record mean for that month. In all the other years, the weakest along-shelf velocity is during January, and increases thereafter. Additionally, the along-shelf velocity during 2007 is the smallest regardless of month.

The spatial variation by month is best represented in figure 22. Lines B and C are typical monthly mean flow patterns. The pattern marked by line B is best described as “veering.” This is when the mean current velocity is strongly in the positive cross-shelf direction over the inner half to three-quarters of the line, and then it begins to turn clockwise. This may be indicative of a convergence in cross-shelf velocity. The pattern in line C is best described as “twisting.” Inshore

of 40 m the current direction is in the positive along-shelf direction, between 40 m and 70 m the velocity is a minimum, and offshore of 70 km the current magnitude continues to increase as the current direction continues to turn clockwise. This may be indicative of a shear flow in the cross-shelf direction.

Daily/ Hourly Variations in the Surface Velocity

Figures 23 and 24 are a visual of the periodicity of current variations, which have been found via spectral analysis to be most energetic at periods of 3 to 4 days. Plotted as such, the cross-shelf variations in velocity components u (cross-shelf) and v (along-shelf) are not easily distinguishable.

To quantify the horizontal velocity variability in u and v , a cross-shelf anomaly was calculated at each time. This was done by calculating the line mean (average of all 25 points on line B) u and v at each hour during which there are surface velocities. Then at each hour, at all the points along that line, the line mean is subtracted from the instantaneous u and v of every individual point. However, when the line mean velocity (figure 25) is subtracted out, cross-shelf regions and time periods of convergence and divergence (figure 26) as well as shear flow (figure 27) stand out. Periods of convergence are identifiable by currents on the outer portion of the line moving inshore while currents on the inner portion of the line move offshore. Periods of shear are identifiable by opposite magnitudes of along-shelf current. These will be used in further analysis later in this work.

Surface Velocity and Wind

Since surface currents in this region are predominately wind-driven (*Ou et al.*, 1981), the next portion of my analysis focused on the cross-shelf variability of wind influence upon surface currents.

A cross-correlation analysis was performed on the spatial mean current and the wind to find that the current lags the wind by one hour. This is in agreement with *Dzwonkowski et al.* (2008a)'s value of 0 - 3 hours for what they define as the mixed period (December - March).

However, the correlation coefficients change by less than 0.01 for a 0 - 3 hour lag range. With these results, in addition to the fact that the velocities are low-pass filtered which makes a one hour lag rather irrelevant, instantaneous wind and current vectors are compared.

First, for each winter, for each point along line B, a complex correlation was performed between the demeaned wind and demeaned surface velocity. From this, a magnitude and phase of correlation, for each point, for each winter was obtained.

The degree to which the cross-shelf variability of the surface velocity is due to wind is visible in figure 28. The wind/current correlation magnitude has a maximum just offshore of 80 km at 0.69 and decreases to approximately 0.49 at 150 km offshore. This is a proxy for the portion of the low-pass filtered current that can be attributed to winds. In these calculations, a positive phase angle is defined as the current being to the left of the wind. Also, the wind/current correlation phase ranges from -60° T to 10° T. It decreases (becomes more to the right of the wind) as depth increases. In the record mean phase there is a plateau around midshelf. Furthermore, the greatest variation in phase between the years is offshore of 90 km. It is important to acknowledge that the flow in this region is not in Ekman dynamical balance, such that the surface velocity would be 45° to the right of the wind. However this is due to the fact that shallower depths are more affected by bottom friction, hence the larger (more negative) phase angle with distance offshore and the current is more Ekman-like.

Then the instantaneous wind-driven velocities at each point for each surface velocity component, u and v were computed. At each point, a linear regression was performed between u and the cross-shelf and along-shelf components of the wind. The same was done for v . From this, coefficients a and b , for u and v respectively, describe the winter mean influence of the wind components at that point. With these coefficients equations (5) and (6) were then used to calculate the instantaneous wind-driven velocity at each point.

$$u_{wind-driven} = a_1 * u_{wind} + a_2 * v_{wind} + a_3 \quad (5)$$

$$v_{wind-driven} = b_1 * u_{wind} + b_2 * v_{wind} + b_3 \quad (6)$$

The residual velocity was calculated by taking the original, low pass filtered u and v and subtracting out the wind-driven velocity, for each point, at each time. The residual is assumed to be

influenced by non-tidal and non-wind forcings, of which include the far-field dynamics.

Figure 29 shows velocity variance, separated into wind-driven and residual components, as function of cross-shelf distance. In subfigures 29a,c,e, g,i and k, it is evident that the wind-driven portion of cross-shelf velocity generally increases with distance offshore. On the other hand, in subfigures 29b,d,f,j and l, it is evident that the wind-driven portion of along-shelf velocity generally decreases with distance offshore. Note the cross-shelf location at which the wind-driven velocity variance is equal to the residual velocity variance. For the cross-shelf velocity variance, the wind-driven portion is at a minimum at 30 km and overtakes the residual portion at 45 km. From that point on, the wind-driven portion tracks with the observed current. For the along-shelf velocity variance, the wind-driven portion has peaks in the inshore regions and linearly decreases as a function of distance offshore. It is around 90 km that the wind-driven portion is less than the residual portion. Note that in 2003 and 2004 there is not a minimum in along-shelf velocity variance (noted by the blue line). This can be attributed to the lower residual (green line) offshore of 120 km.

Regardless of year, winds are most frequently in the positive cross-shelf direction, particularly between 90°T and 140°T (figure 30). Not only are winds from this direction more frequent, but they are 3 m/s stronger wind speed on average. A second band for more frequent winds is towards the NNE, between 10°T and 40°T . Note that distribution of wind direction in 2006 and 2007 is most similar and in agreement with *Saunders* (1977) assessment of typical wind direction. Also note that 2003 - 2005 have higher occurrences of winds to SE (200°T and 230°T).

3.3 Comparisons

This section analyzes the temporal and spatial relationships between front location, surface velocities, wind and heat flux. It will discuss the features found using the aforementioned data, in the vicinity of the 30 m and 50 m isobaths, and how they seem to relate to one another.

Cross-shelf Convergence

Along line B, there appears to be a positive correlation between surface velocity gradients and front probability. The seasonal mean divergence was calculated at each point along line B. The offshore distance at which the winter mean velocity is convergent (negatively divergent) is coincident with the offshore distance at which there are increased front probabilities (figure 31). Generally there is a band of convergence along the 30 isobath and offshore of the 50 m isobath. However, this does not entirely hold for all years, in particular, 2003. From equation 2 it is evident that when there is convergent flow, horizontal gradients (in this case $\frac{\partial T}{\partial x}$) increase. Because front data is rather intermittent, an approximation of the effect of convergence on an instantaneous space and time is difficult. However, over the course of the season, the effect of convergence can be estimated from the record SST gradient magnitude (figure 14b), which is $0.25^{\circ}\text{C}/\text{km}$ and mean SST gradient direction (figure 15), which is 105°T . From this $\frac{\partial T}{\partial x}$ and $\frac{\partial T}{\partial y}$ are calculated to be $0.23^{\circ}\text{C}/\text{km}$ and $0.098^{\circ}\text{C}/\text{km}$ respectively. In the vicinity of the 30 m and 50 m isobath, the seasonal divergence (figure 31), $\frac{\partial u}{\partial x}$, is approximately $-1 \cdot 10^{-6} \text{ s}^{-1}$ and the seasonal vorticity (not shown), $\frac{\partial v}{\partial x}$ is approximately $-1 \cdot 10^{-6} \text{ s}^{-1}$. Assuming

$$\frac{d}{dt} \left(\frac{\partial T}{\partial x} \right) \approx - \frac{\partial u}{\partial x} \frac{\partial T}{\partial x} \quad (7)$$

then the rate of change in cross-shelf temperature gradient due to convergence is $2.3 \cdot 10^{-7} \text{ }^{\circ}\text{C}/\text{km}/\text{s}$. And in one day, the convergence could change the temperature gradient by $+0.20^{\circ}\text{C}/\text{km}$.

Assuming

$$\frac{d}{dt} \left(\frac{\partial T}{\partial x} \right) \approx - \frac{\partial v}{\partial x} \frac{\partial T}{\partial y} \quad (8)$$

then the rate of change in cross-shelf temperature gradient due to shear is $9.8 \cdot 10^{-8} \text{ }^{\circ}\text{C}/\text{km}/\text{s}$.

And in one day, the negative shear/vorticity could change the temperature gradient by $+8.5 \cdot 10^{-3}$

°C/km. Given these values for $\frac{d}{dt} \left(\frac{\partial T}{\partial x} \right)$, convergence is more influential than shear. Furthermore, a sustained convergence can double the existing gradient (0.25°C/km) in approximately 1.25 days. However, it takes about 30 days of shear/vorticity to cause the existing gradient to double.

Composite Analysis

The determination of changes in front location and strength are rather limited, due to cloudiness. Discussed below are three one to two month periods during which fronts were observed along the 30 m and 50 m isobaths. Shown in these figures are wind speed and direction, cross-shelf velocity anomaly, along-shelf velocity anomaly, front location, percent clear in Box 30 and Box 50. The example periods are January 28 - March 18 2003, December 1 - December 31 2005, and February 1 - February 28 2007.

In winter 2003, it is evident that winds to the S to SW results in strong convergence in the cross-shelf velocity anomaly, at midshelf (figure 32b). This is most distinguishable from January 29th to February 2nd, from February 15th to February 19th, and from February 26th to March 2nd. Note that it is frequently cloudy during these periods. But, once the percent clear increases after these incidents, fronts become apparent. There are times when the cross-shelf location of maximum convergence (blue offshore and red inshore) is coincident with the cross-shelf location of maximum shear.

In December 2005, periods of sustained cross-shelf convergence are less frequent and more inshore (figure 33) than in the previous example. But there is a consistent shear in the along-shelf velocity, particularly during the latter one third of the month that is coincident with fronts along the 50 m isobath.

The last example (figure 34) includes the "Upshelf Incident," which takes place between February 2 - 18th 2007. This example is the most distinct in showing 50 m isobath fronts in the vicinity of shear in the along-shelf anomaly. Cross-shelf variations in cross-shelf anomaly in this example are coincident with 30 m and 50 m isobath fronts.

Heat flux, Wind, and Fronts

Another factor affecting SST gradient magnitude, which we will discuss briefly, is heat flux (sum of latent and sensible heat fluxes). The winter mean heat flux during 2005 and 2006 are above average/record mean, which translates to less heat flux out of the ocean surface (figure 35a). In figure 35b it is evident that the relatively more positive monthly mean heat flux of January 2006 results in the higher winter mean. As for the 2005 winter mean, all four winter months tend to be approximately greater than or equal to the record mean monthly heat flux.

On a month to month basis, over the record, heat flux in Box 50 is inversely related to SST gradient magnitude in Box 50 (figure 36). However, there appears to be no relationship between these two variables in Box 30. Since shallower depths cool more quickly, it would have been expected that SST and heat flux in Box 30 would be correlated.

For SST gradient magnitude the anomalous year is 2007 (figure 13) during which the winter mean in Box 30 is less than the winter mean in Box 50. This is likely due to an extended period of strong winds towards the ESE which cooled the entire shelf.

During March wind strength typically decreases and winds to the W to NW become more common (not shown). This is believed to be influential in 50 m isobath fronts moving inshore. Extended periods of winds to the S (as was the case during February 2005) lead to an increased region and period of convergence along the 30 m isobath. It is unclear whether this wind regime either dissipated fronts along the 50 m isobath or forced them inshore. I have more confidence in the former suggestion, given that the SST gradient magnitude of fronts in Box 50 are the lowest magnitude in 2005, with respect to all years and both boxes (figure 13).

4 Discussion and Conclusions

It is difficult to distinguish the exact time, movement, and consequently the cause of the fronts due to the short periods with which they form or decay largely due to cloudiness. There is significant variability from year to year. Though varying in time, space, orientation, and strength over a season, as well as over the five year record, winter fronts are located just offshore of the 30 m and 50 m isobaths. It is still unclear as to the entire dynamical picture, but I believe the surface currents are a major forcing function in front positioning and strength. It was theorized that a geostrophic surface jet is co-located with fronts, but there is no evidence of that. If a jet does occur, either it is narrower than the 6 km CODAR resolution can distinguish or it is subsurface. There does seem to be a wider region of strong down-shelf flow, $O(20 \text{ km})$ wide offshore of the 50 m isobath, just at the conclusion of the "Upshelf Incident."

Also, the record mean change in front location offshore over the four winter months is less than 5 km. Though it was found by *Ullman and Cornillon* (2001) that midshelf fronts progress offshore over the winter months, the data here are incongruent with that finding. This discrepancy may be due to the difference in the geographical extent of my analysis compared to *Ullman and Cornillon* (2001). Their region covered the entire shelf width and a further extent in the along-shelf direction, rather than 25 km by 200 km boxes around specific isobaths.

Furthermore, the bathymetry in this region is gently sloping and upon cursory analysis it does not appear that fronts are coincident with high bathymetry gradients. There is a great deal of noise in the daily mean front location data (figure 11) displaying the fronts have significant variability in position. I am not convinced that relatively high bathymetry gradient regions of the shelf are where fronts occur, as claimed by *Ullman and Cornillon* (2001) and *Gong et al.* (2006).

Similarly, there is no evidence of fortnightly or monthly movement of front location, as is evident by the spectral analysis results, that would support *Ou's* theory. Furthermore, *Ou* argued that a minimum in tidal diffusivity times depth would result in a maximum in density gradient at midshelf. There are minima found in the plots of velocity variance as a function of cross-shelf distance. However, since the surface velocities were low-pass filtered it is unlikely that this is related to tidal diffusivity. Despite this fact, it should not be neglected that this could be another

form of diffusivity.

It is also important to note that the range of SST gradient magnitudes (0.23 °C/km to 0.32 °C/km) found in this work are comparable to those found for winter fronts in Taiwan Strait (Chang *et al.*, 2006).

In terms of forcing in the cross-shelf, offshore (positive cross-shelf) winds seem to be correlated with stronger fronts, expressed as higher SST gradient magnitudes. In the case of 2007, when the fronts are stronger in the 50 m isobath region, this is likely due to the relatively longer period of sustained winds to the SE that cooled the shelf more rapidly and farther out than in the previous four years. Also Oey (1986) asserts that the number of COA outbreaks within a given season determine the presence of a midshelf front. The daily mean heat flux time series during 2006 (not included) leads us to believe that there were fewer periods of increased negative heat flux, and that is a factor in the fewer fronts at the 30 m isobath. By the same token, fewer fronts on the 50 m isobath during 2005 are likely a result of the weaker (more positive) winter mean heat flux, in addition to other factors.

Another factor I think resulted in fewer fronts on the 50 m isobath during 2005 is strong negative along-shelf surface velocity. Csanady (1978) asserts that fronts are strengthened by down-shelf surface flow. However, strong along-shelf velocities seem coincident with either weakened or migrated (towards inshore) 50 m fronts in February and March 2005 as well as in March 2004.

Winds to the SW lead to cross-shelf convergence at the 30 m isobath, while winds to the SE lead to convergence at the 50 m isobath. Shear appears to be a contributing factor to front location and orientation. In all, Hoskins (1982) theory appears to be the prominent mechanism behind why fronts are sharpened along the 30 m and 50 m isobaths. It appears as though a sustained convergence can solely generate a typical MSF SST gradient (0.25°C/km) in 30 hours. And a sustained negative shear/vorticity can solely generate a typical MSF SST gradient (0.25°C/km) in 30 days.

If these two fronts are type 1 as described by Ou *et al.* (1981), then there is not simply a single causation that determines their formation. There is much more in terms of coastal

dynamics and mesoscale processes that come into play, particularly the vertical structure and the influence of the far field, that make it difficult to state with certainty the relationship between surface fronts and surface currents.

4.1 Ongoing Research

Researchers at Rutgers University and the University of Rhode Island have a wealth of information in this region at their disposal. They are able to capture a more complete spatial and temporal resolution of these fronts from moored and shipboard Acoustic Doppler Current Profilers (ADCPs), Autonomous Underwater Vehicles (AUVs), thermistors, as well as from satellites and CODAR. Further studies should incorporate as many of these data sets, and particularly those that are able to characterize front location on a timescale on the order of several days.

There is further work being done by two graduate students, who are analyzing this region over shorter timescales. Both students, in fact, examine the beginning of January through the beginning of April in 2007. One is looking at the hydrological variations in 3D field, while the other is tracking Radium isotopes as a measure of cross-shelf flux.

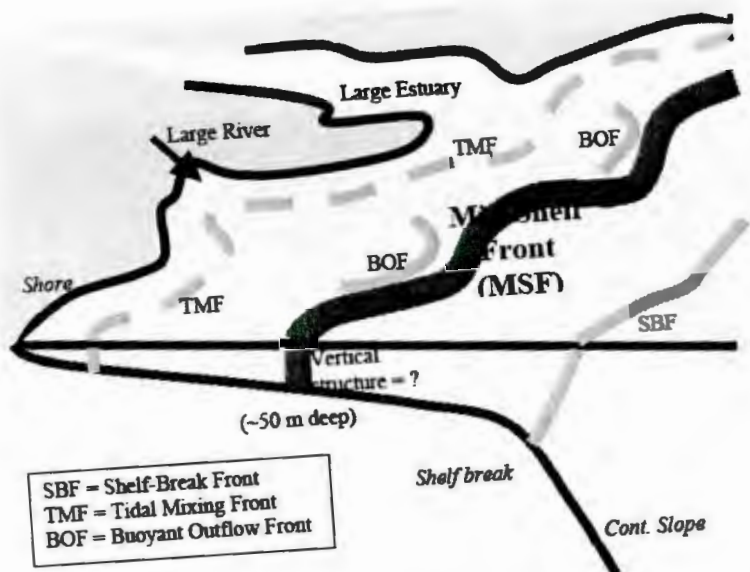


Figure 1. Geographic Location of Various Types of Fronts that occur on the New Jersey Shelf

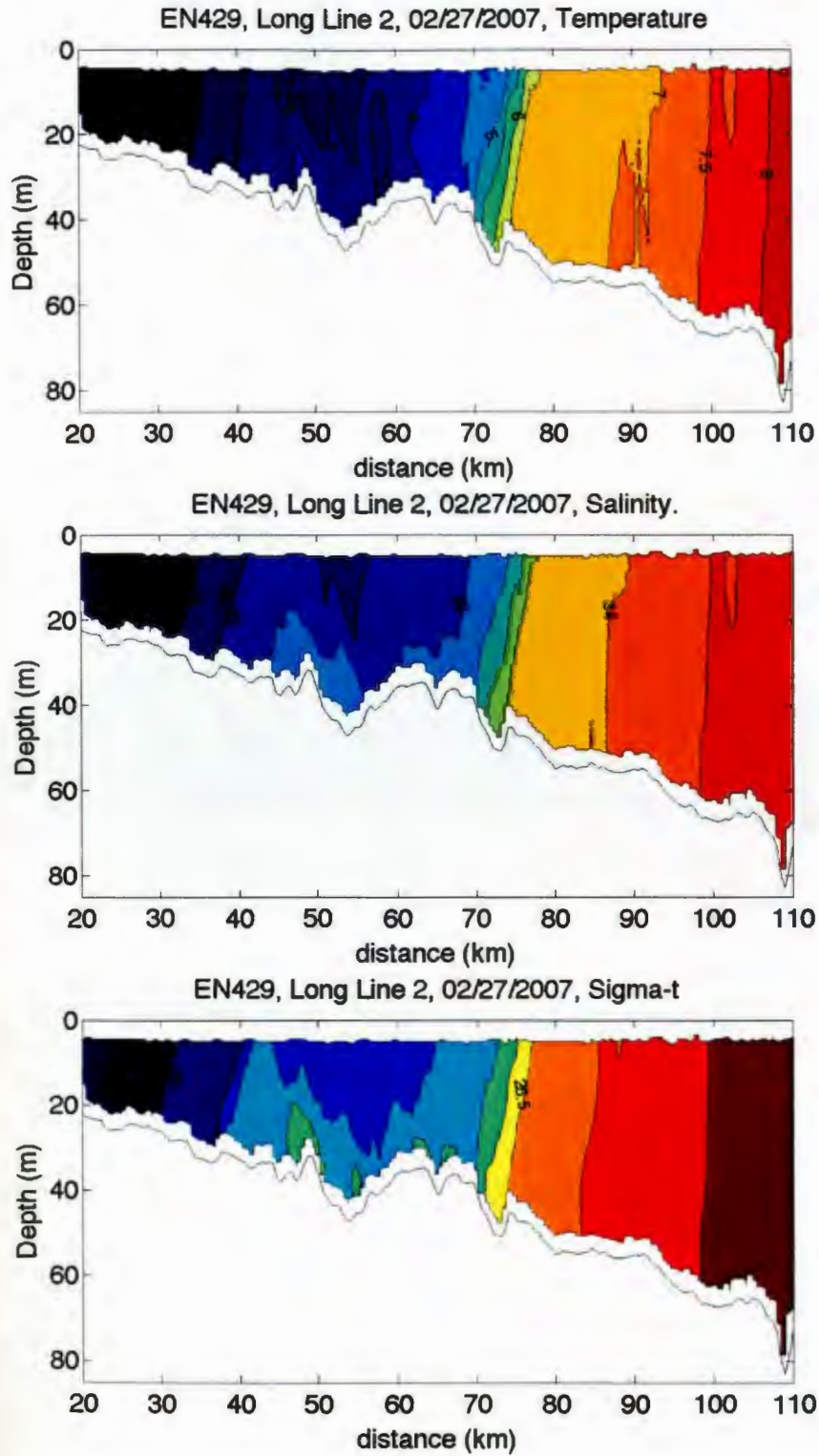


Figure 2. **Midshelf Front Hydrography:** Example from towed CTD transect on February 27, 2007 a) Temperature (°C) b) Salinity c) Density (kg/m³)

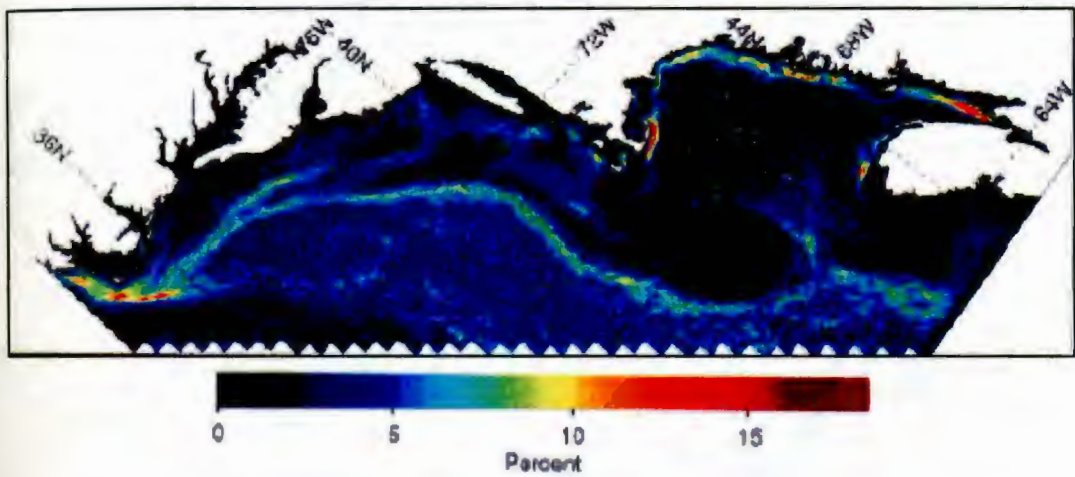


Figure 3. **Previous Detection of Fronts in Middle Atlantic Bight: Percent Front Probability** using AVHRR SST imagery and an edge-detection algorithm. Composite of winters (January-March) 1985-1996, taken from *Ullman and Cornillon (2001)*

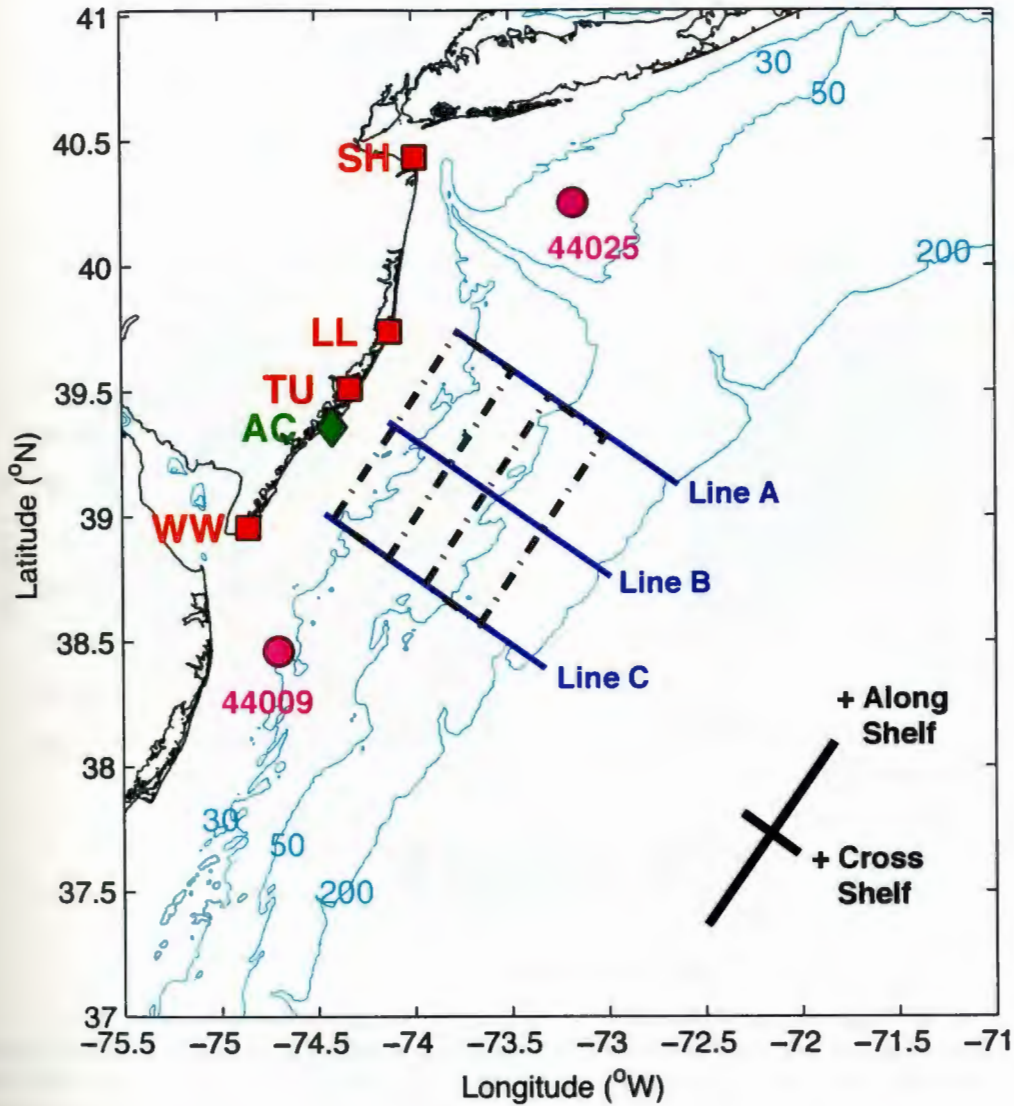


Figure 4. Shelf region of southern New Jersey: The 30 m, 50 m, and 200 m isobaths are shown in cyan. CODAR Stations are shown as red squares: Sandy Hook (SH), Loveladies (LL), Tuckerton (TU), and Wildwood (WW). The Atlantic City (AC) tide-gauge is marked as a green diamond. NDBC buoys are marked by magenta circles. The 120 km Cross-shelf lines A, B, and C are noted in dark blue. The isobath boxes Box 30 and Box 50 (each 100 km by 30 km) are marked with black, dashed lines.

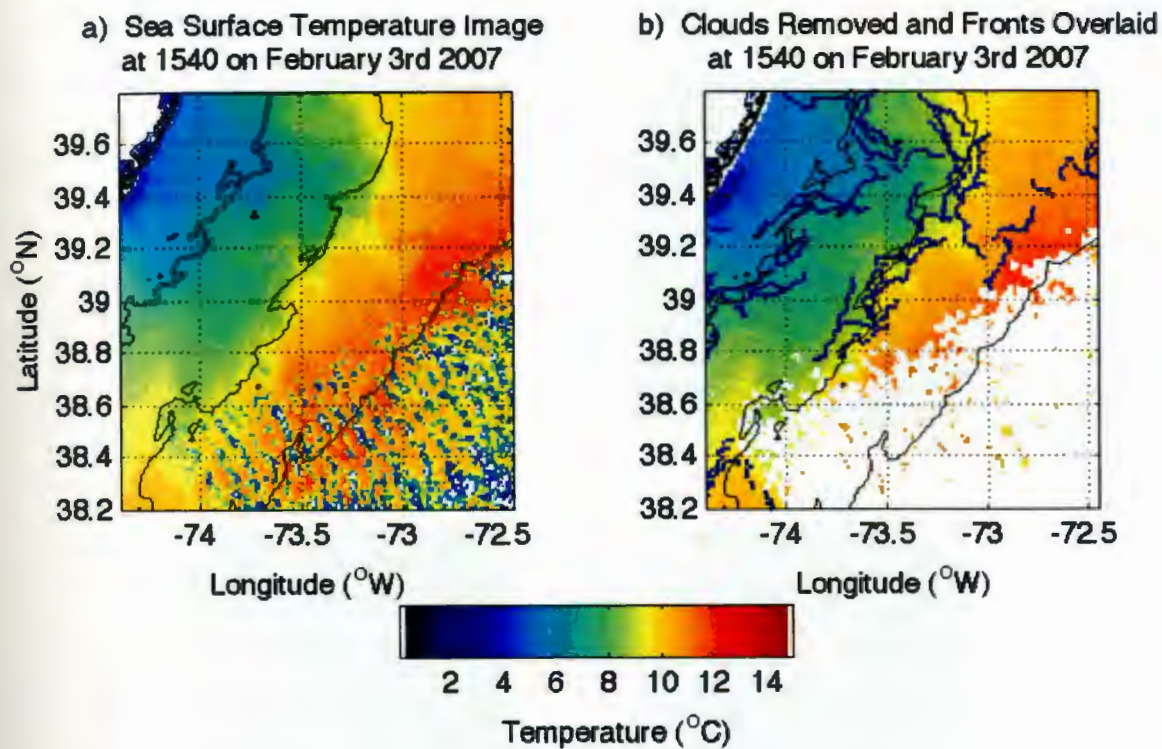


Figure 5. **Sea Surface Temperature Image Processing:** Example image captured by TERRA satellite on 1540 at February 3rd, 2007 a) Sea Surface Temperature b) Same image with clouds removed and fronts found by edge-detection algorithm overlaid.

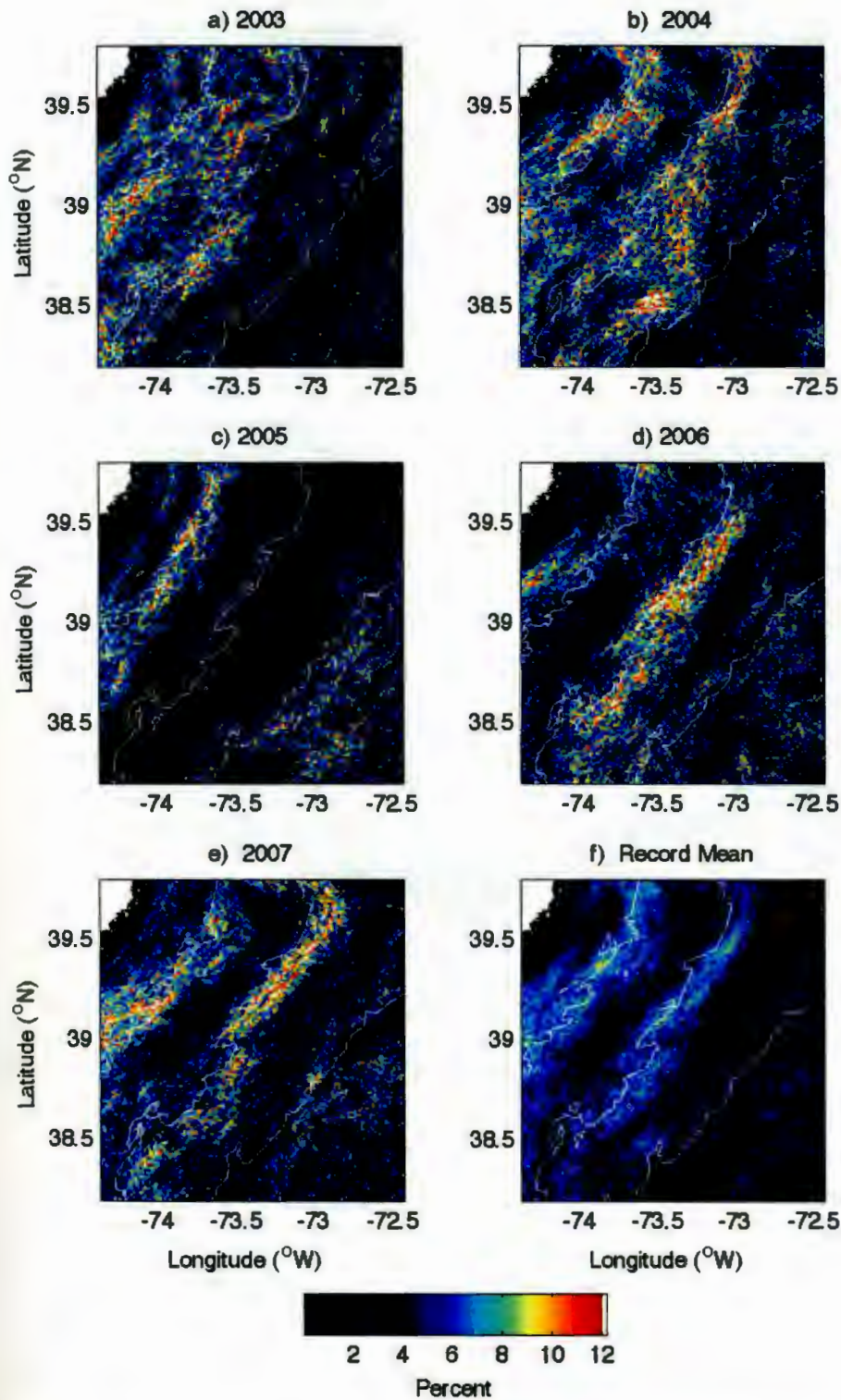


Figure 6. Annual Variation in Winter Front Probability: Winters (December-March) 2003-2007 a) 2003 b) 2004 c) 2005 d) 2006 e) 2007 f) five year record mean. The 30 m, the 50 m, and the 200 m isobaths are denoted in by thin white lines. Pixels with less than 4% probability were masked for clarity of viewing.

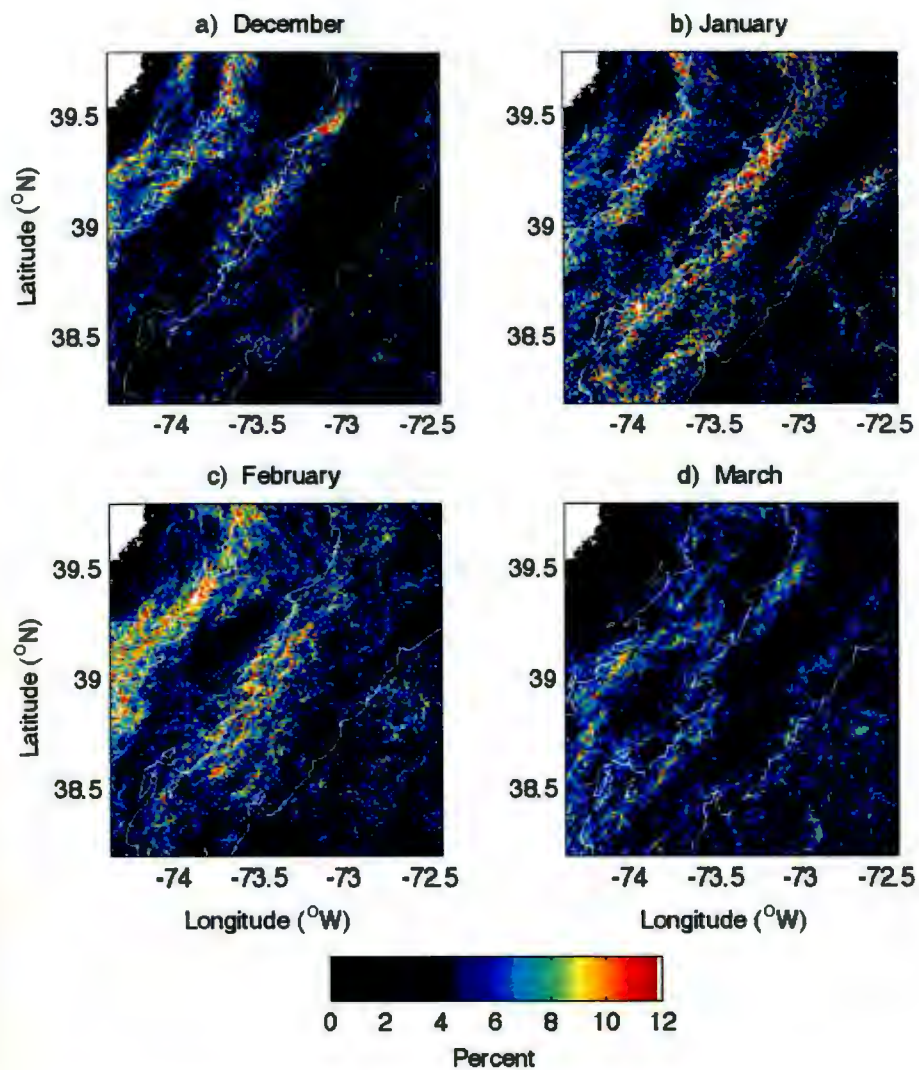


Figure 7. Monthly Variation in Front Probability: Five year record mean of a) all Decembers b) all Januaries c) all Februarys d) all Marchs. The 30 m, the 50 m, and the 200 m isobaths are denoted in by thin white lines. Pixels with less than 4% probability were masked for clarity of viewing.

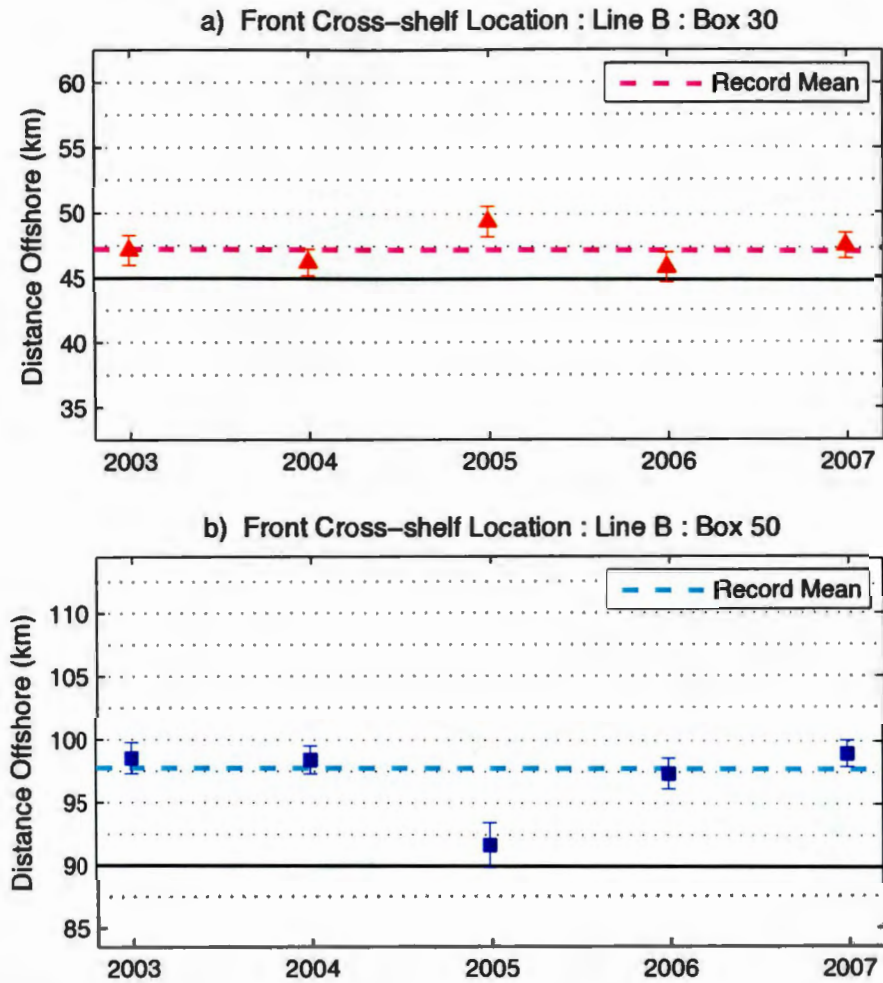


Figure 8. Annual Variation in Front Cross-shelf Location on Line B: Winters (December-March) 2003-2007 and Five year Record Mean a) Box 30 b) Box 50. The solid black lines at 45 km and 90 km denote the 30 m and 50 m isobaths.

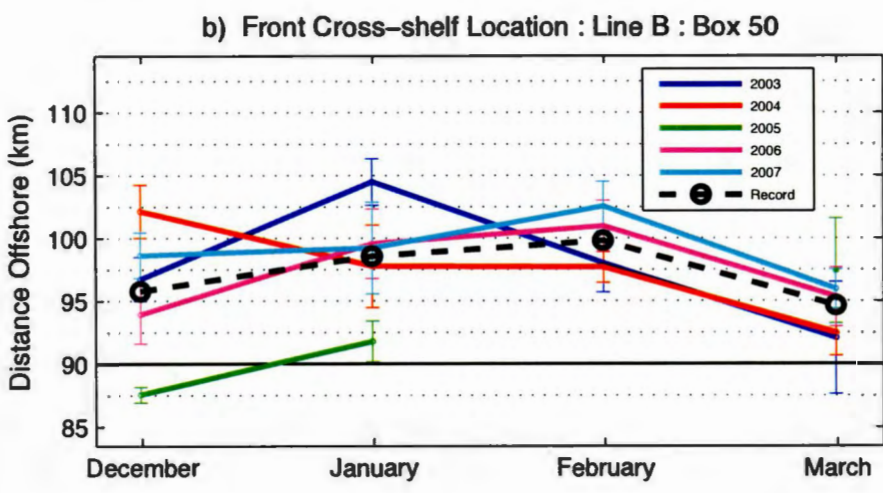
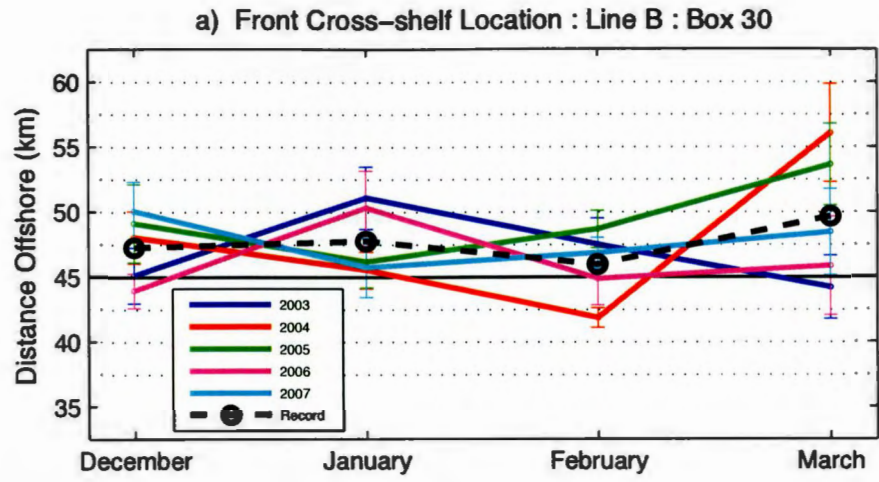


Figure 9. Monthly Variation in Front Cross-shelf Location on Line B: Winters (December-March) 2003-2007 and five year record mean. a) Box 30 b) Box 50. The solid black lines at 45 km and 90 km denote the 30 m and 50 m isobaths.

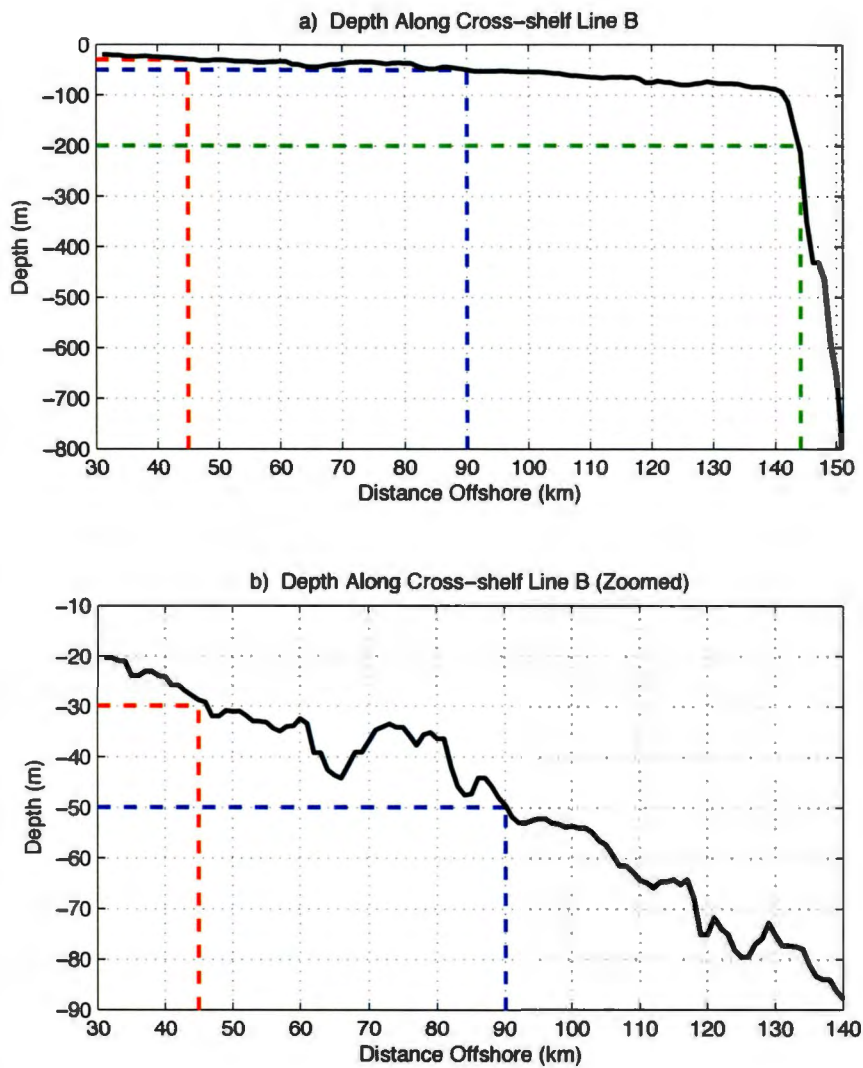


Figure 10. Cross-shelf Bathymetry of Line B : a) Depth versus Distance Offshore : Line B b) Same bathymetry, but inshore of 90 m isobath.

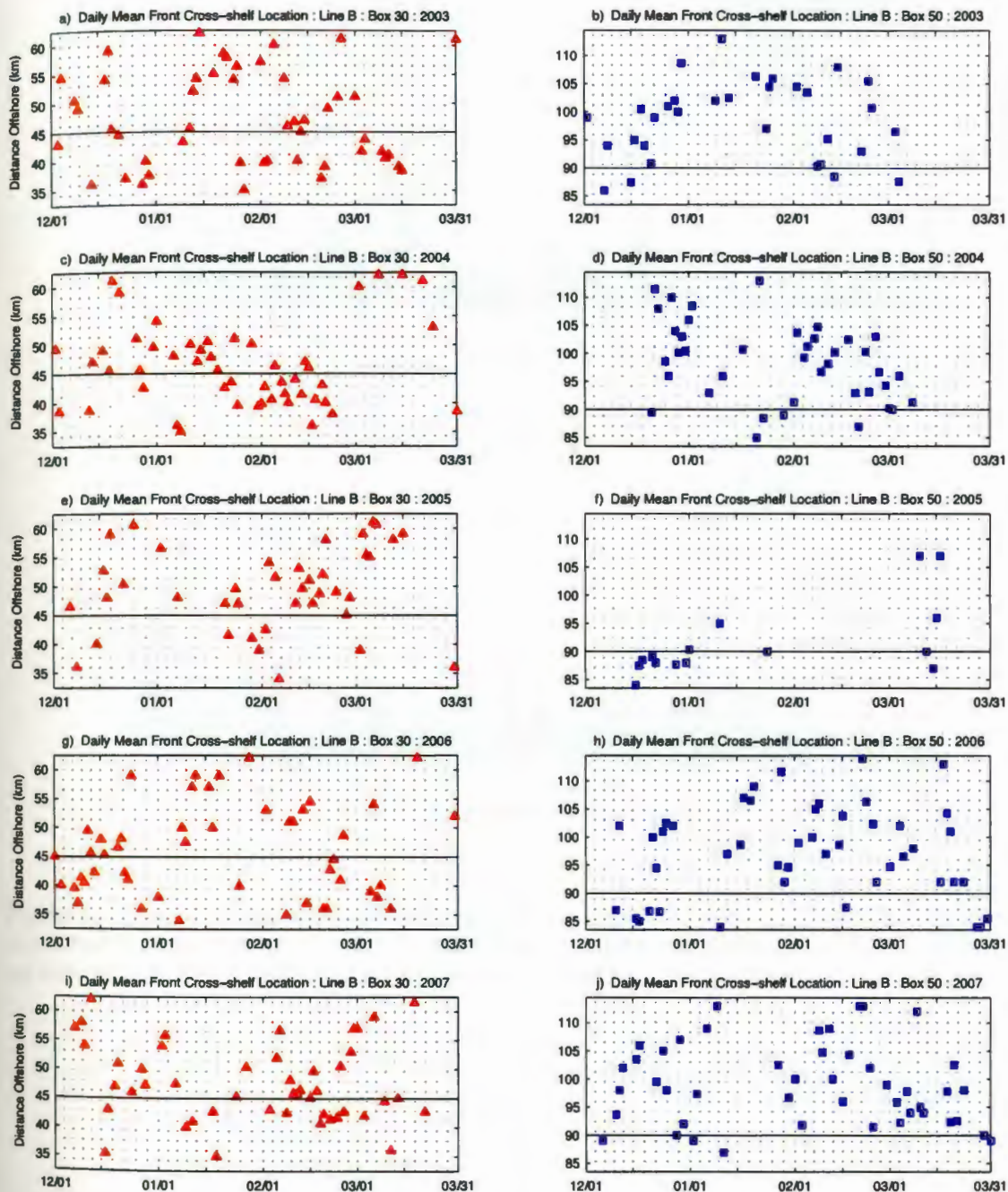


Figure 11. **Daily Variation in Front Cross-shelf Location:** Winters (December-March) 2003-2007. a),c),e),g) and i) Box 30 b),d),f),h), and j) Box 50. The solid black lines at 45 km and 90 km denote the 30 m and 50 m isobaths.

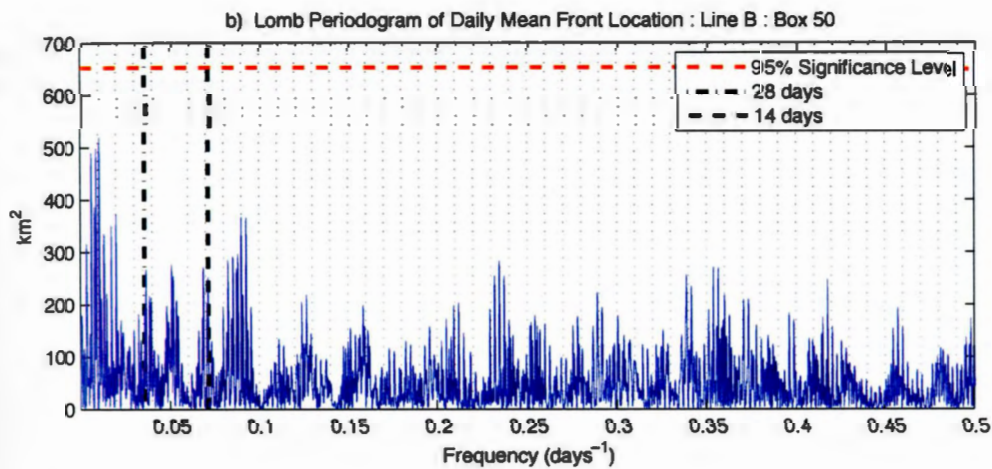
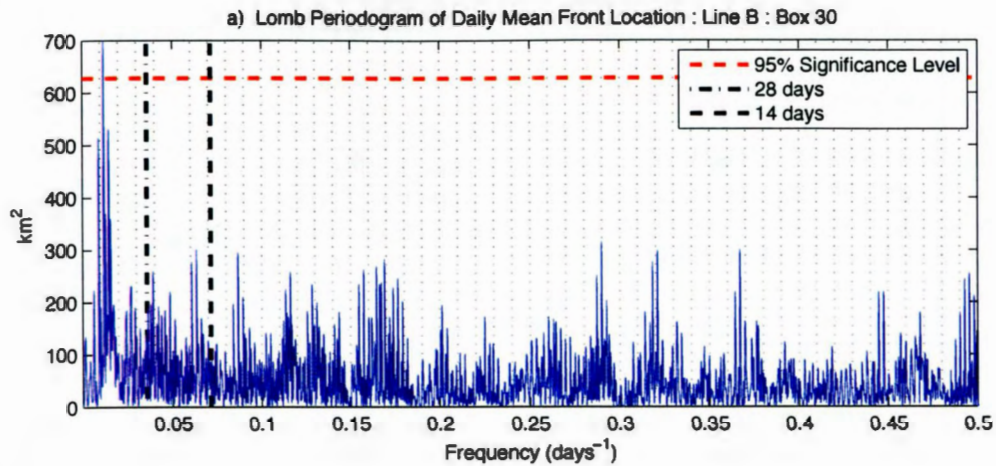


Figure 12. Lomb Periodogram of Front Cross-shelf Location: Spectral analysis performed on five year record to test Ou's theory of front location as a function of tidal amplitude a) Box 30 b) Box 50. The red horizontal dashed lines are the estimated significance level for spectral estimates.

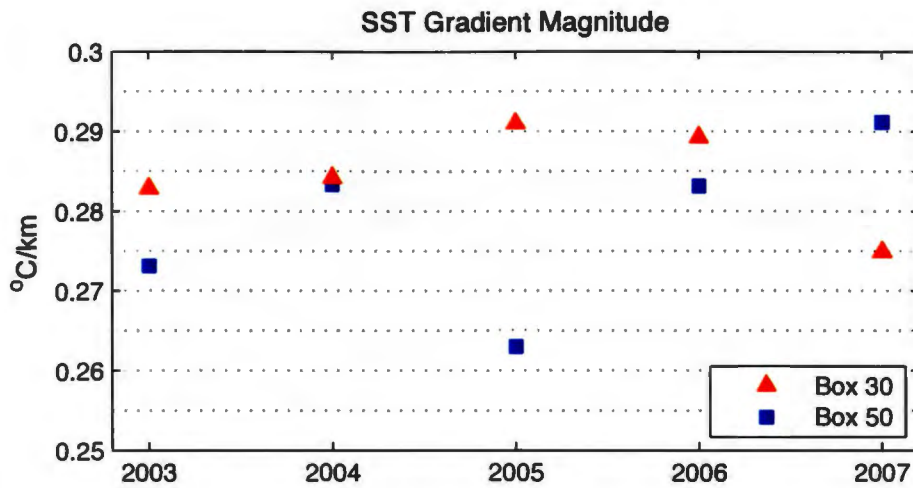


Figure 13. Annual Variation in SST Gradient Magnitude: Winters (December-March) 2003-2007 and five year record mean.

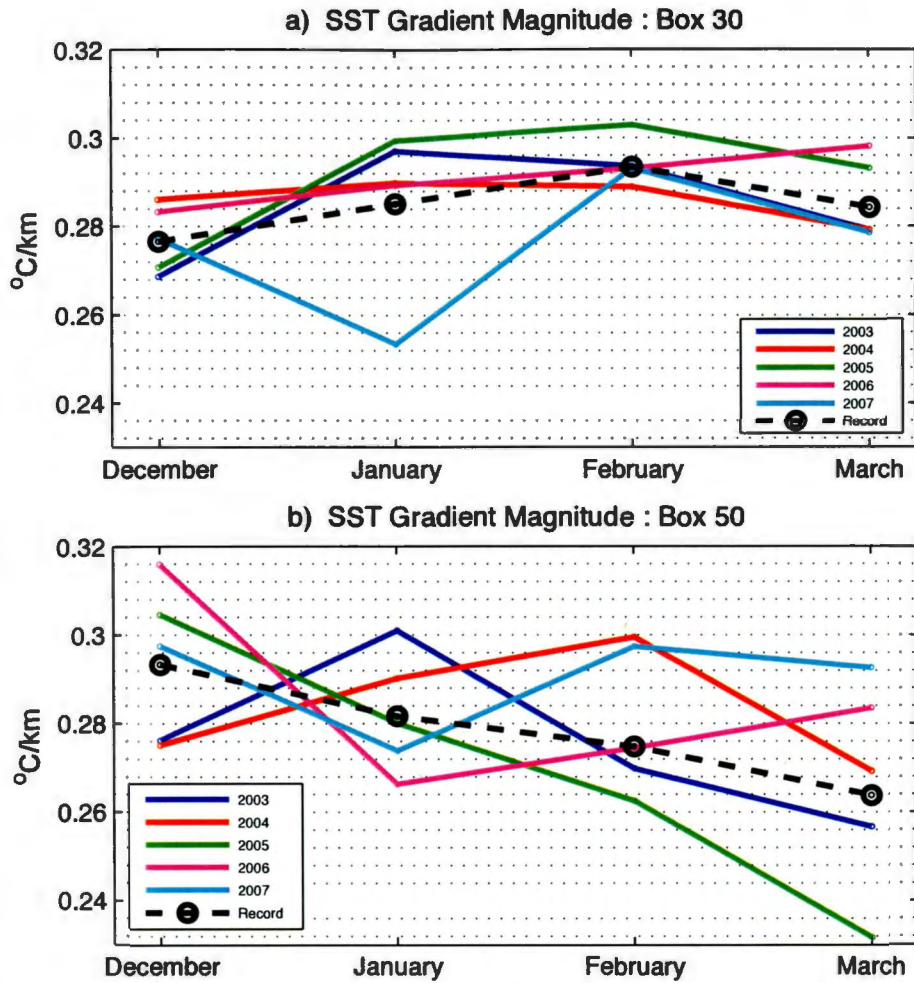


Figure 14. Monthly Variation in SST Gradient Magnitude: Winters (December-March) 2003-2007 and five year record mean. a) Box 30 b) Box 50.

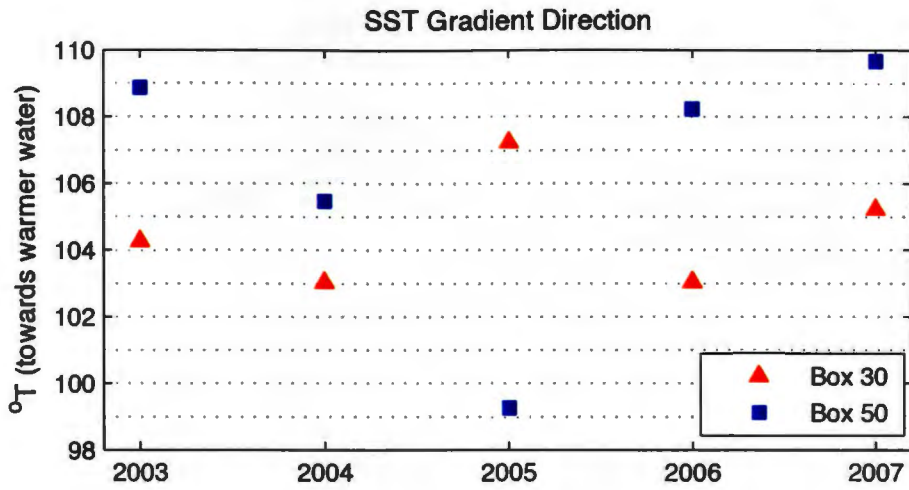


Figure 15. Annual Variation in SST Gradient Direction: Winters (December-March) 2003-2007 and five year record mean.

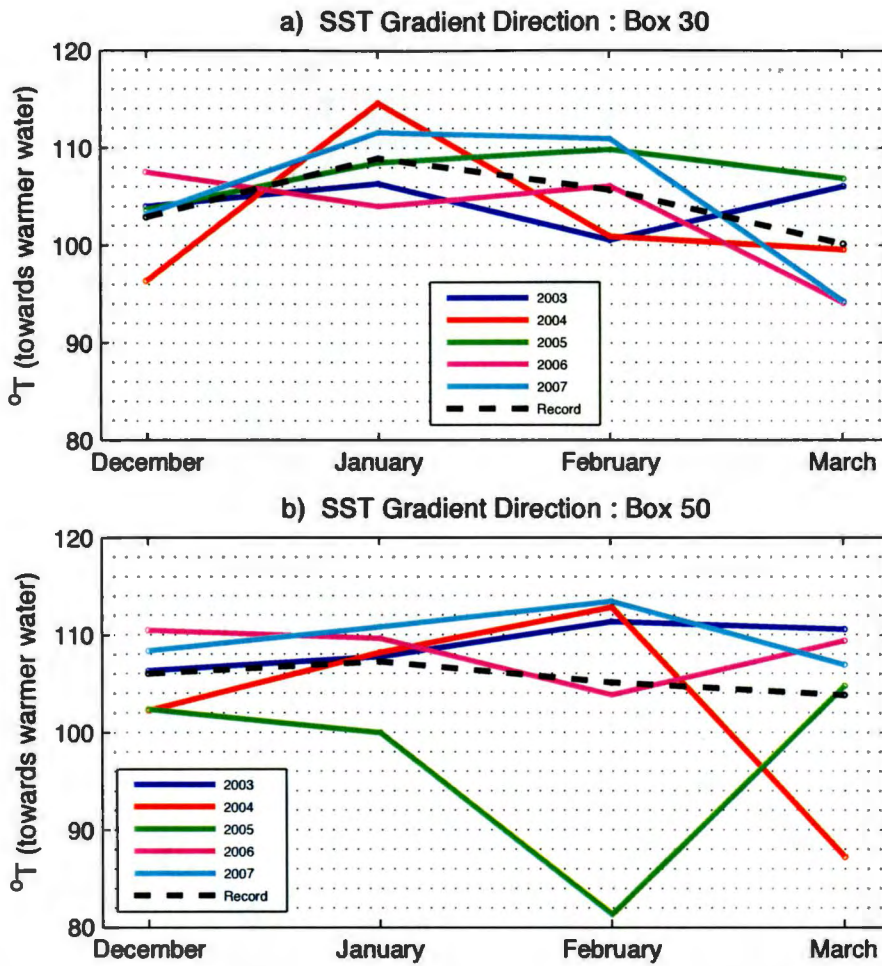


Figure 16. Monthly Variation in SST Gradient Direction: Winters (December-March) 2003-2007 and five year record mean. a) Box 30 b) Box 50.

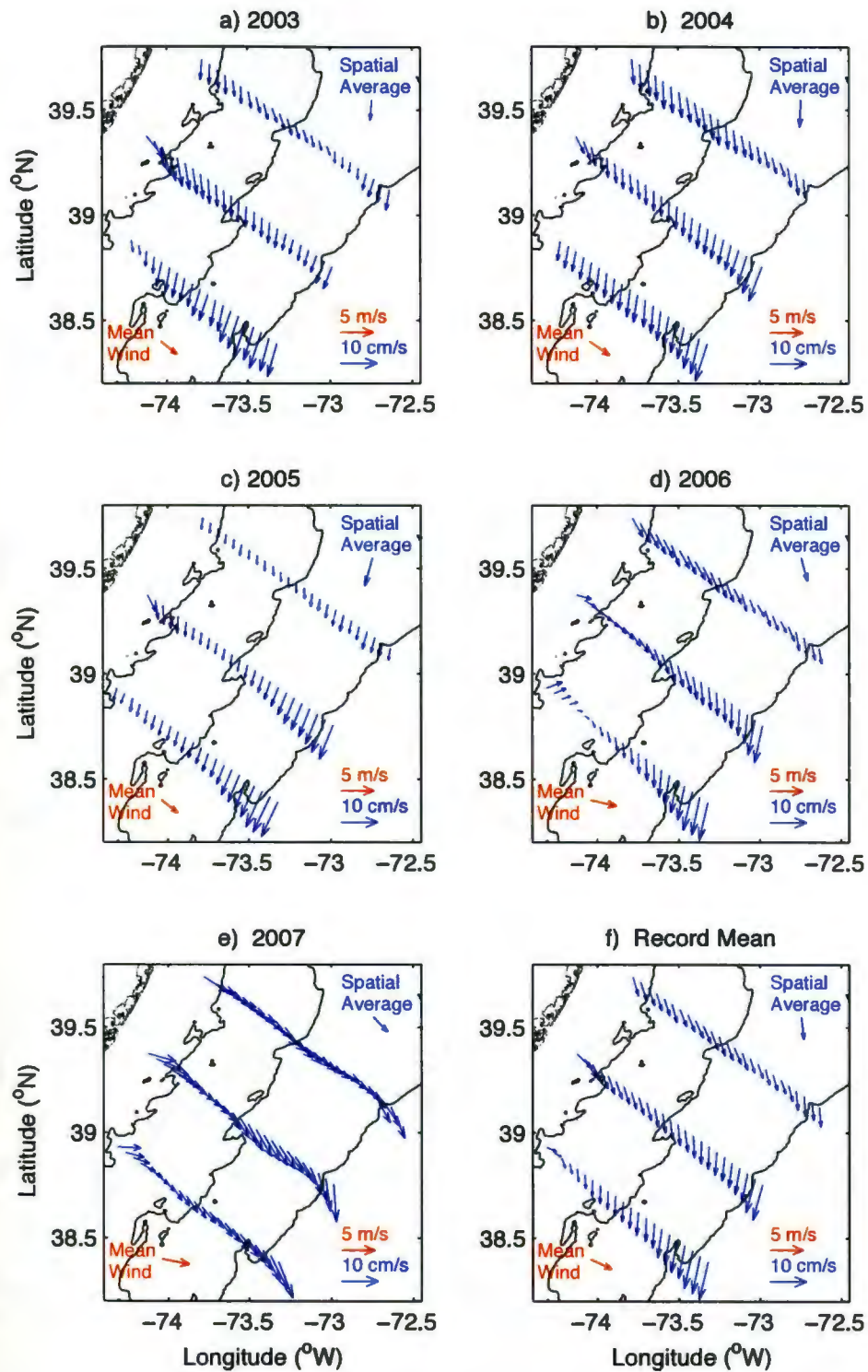


Figure 17. Winter Mean Current Velocity: Winters (December-March) 2003-2007 a) 2003 b) 2004 c) 2005 d) 2006 e) 2007 f) Record Mean

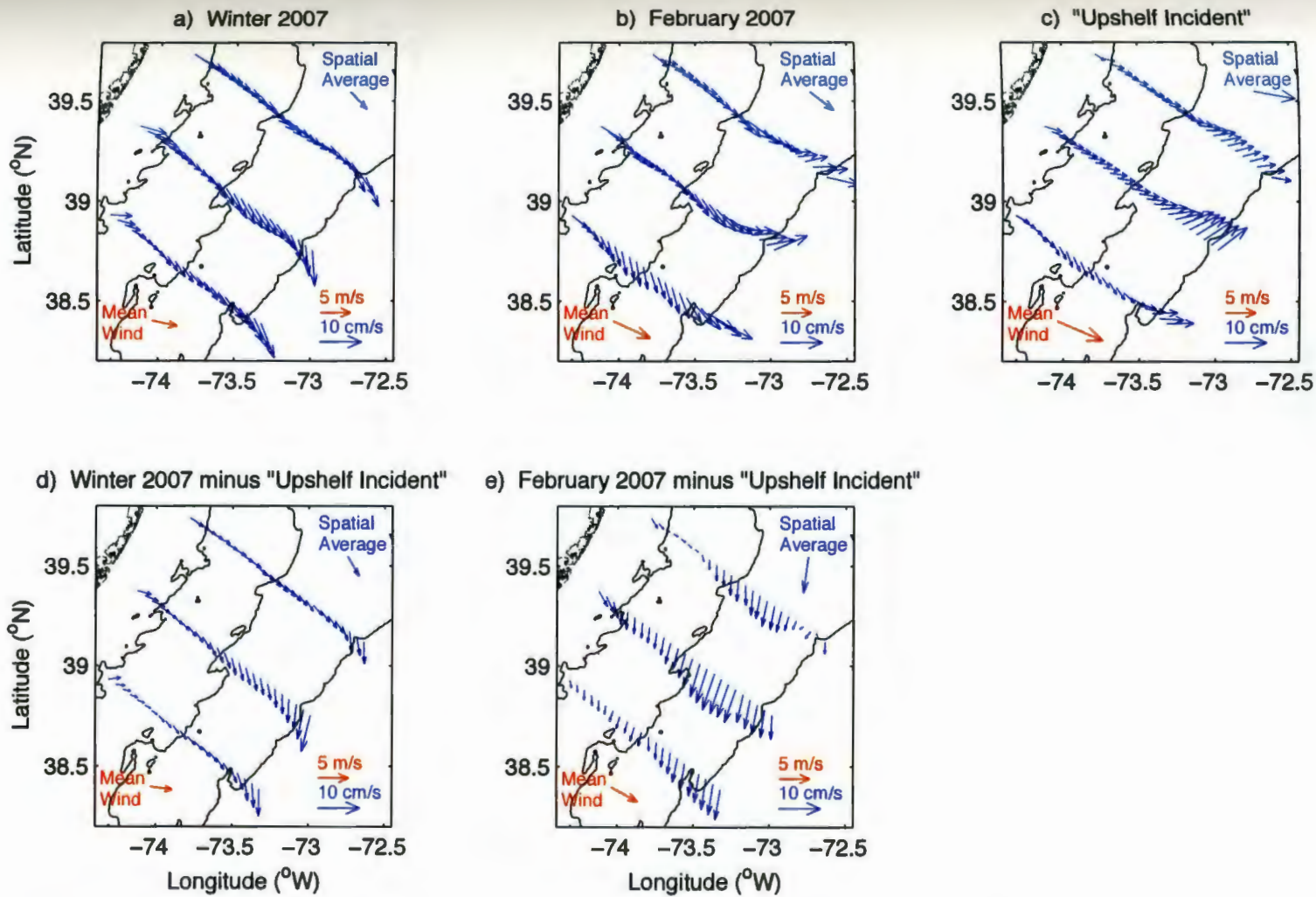


Figure 18. **Upshelf Incident:** a) Winter 2007 b) February 2007 c) February 2nd-18th 2007 d) Winter 2007 minus "Upshelf Incident" e) February 2007 minus "Upshelf Incident"

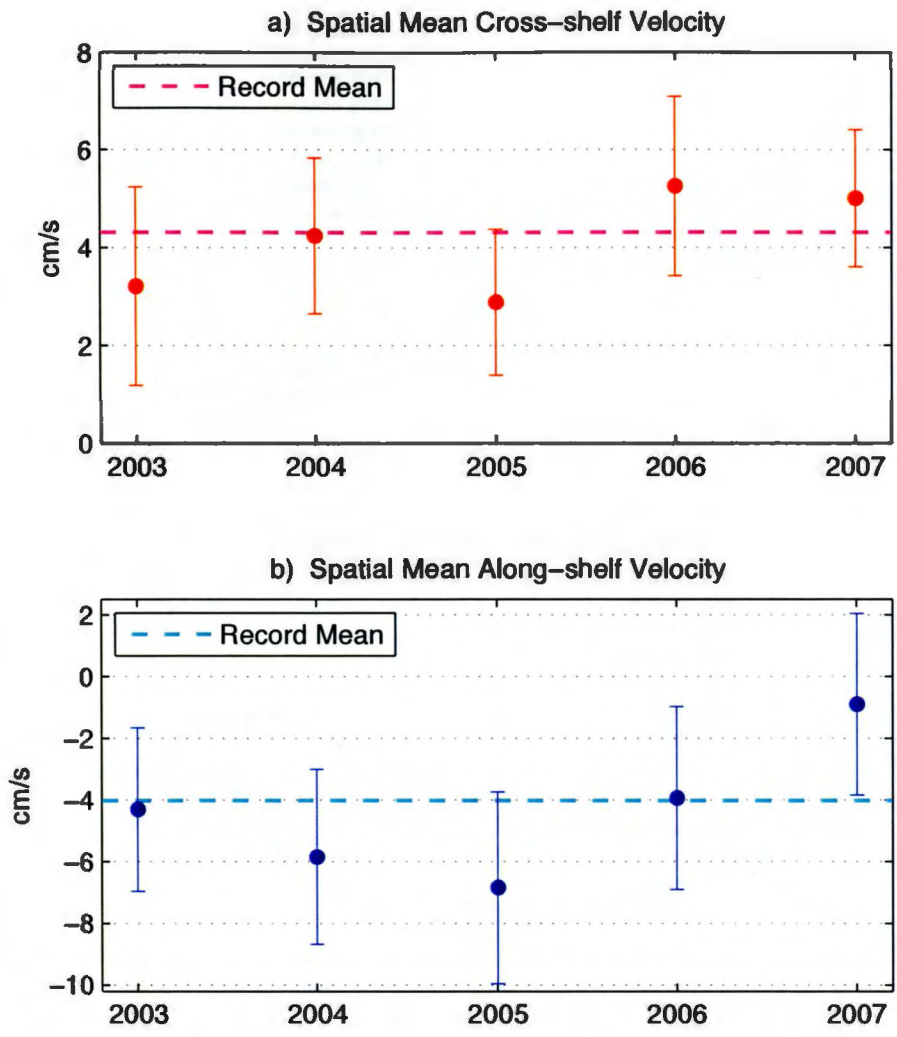


Figure 19. Winter Spatial Mean Current Components: Winters (December-March) 2003-2007 includes Lines A, B, and C a) Cross-shelf Velocity b) Along-shelf Velocity The errorbars mark the standard error of the mean.

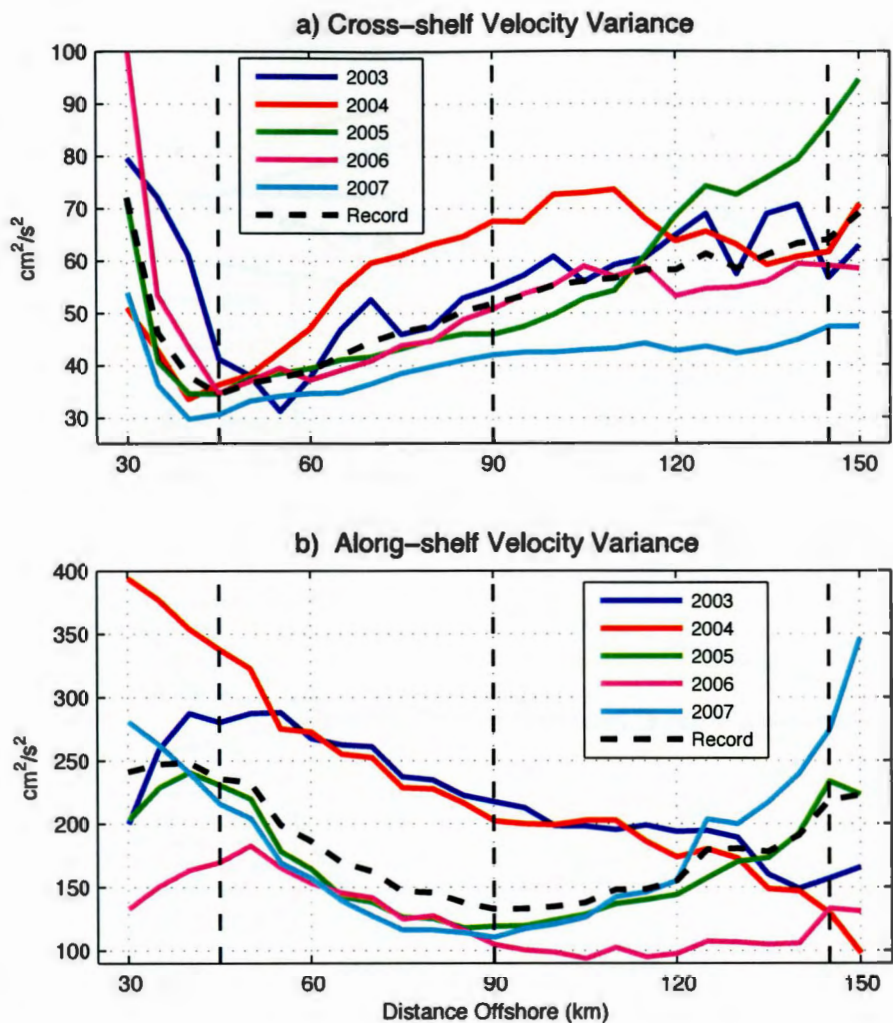


Figure 20. Velocity Variance as a function of Distance Offshore: Line B : Winters (December-March) 2003-2007 and Record Mean a) Cross-shelf Velocity Variance b) Along-shelf Velocity Variance The vertical, bold, dashed, black lines denote the 30 m, 50 m, and 200 m isobaths.

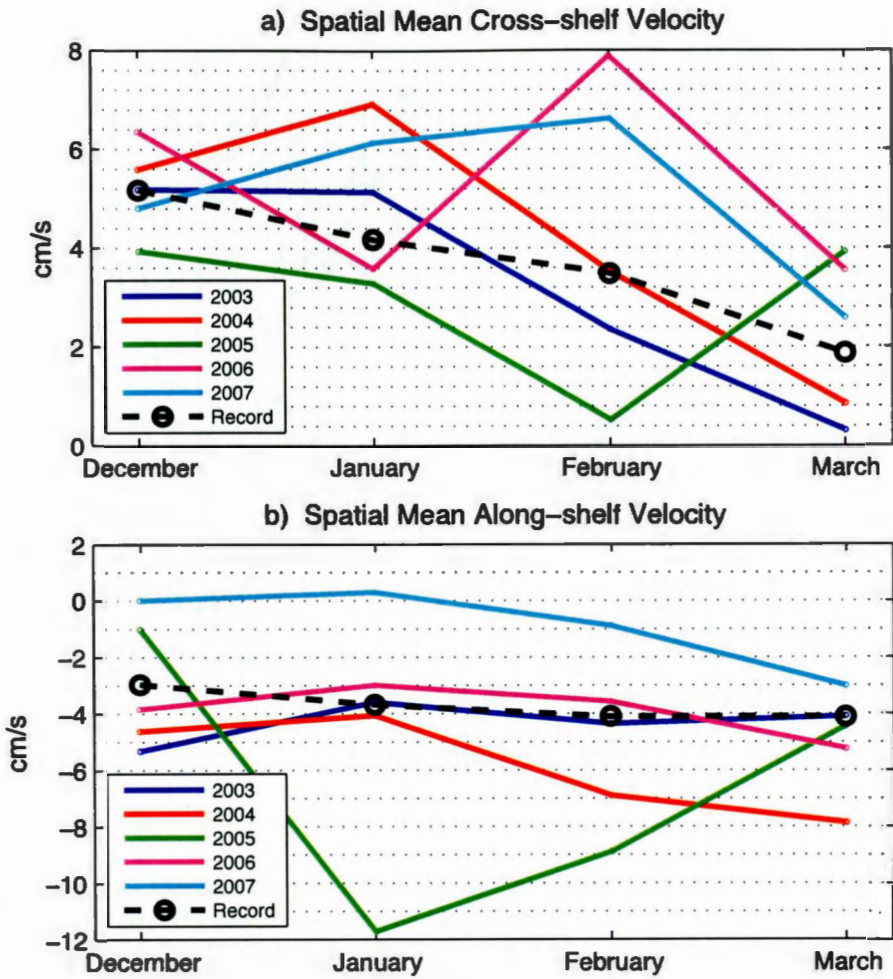


Figure 21. Monthly Spatial Mean Current Components: Winters (December-March) 2003-2007 and Record Mean and includes Lines A, B, and C a) Cross-shelf Velocity b) Along-shelf Velocity

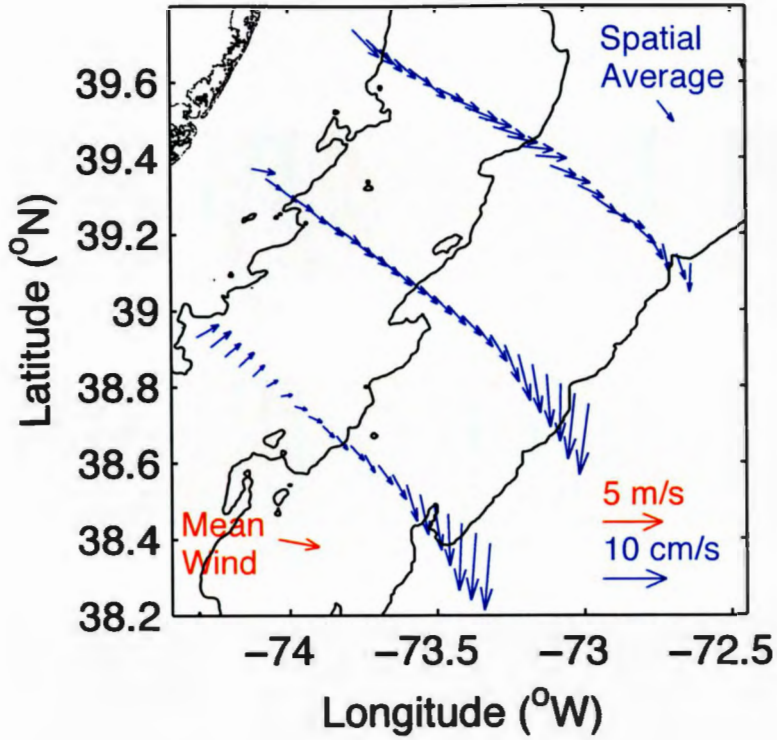


Figure 22. **Shelf-wide Current Direction Variations:** The monthly mean velocity field during December 2005 marks two patterns seen in the surface flow fields. Line B (the middle cross-shelf line) is an example of the “veering” pattern, and line C (the southern most line) is an example of the “twisting” pattern.

Cross-shelf Velocity

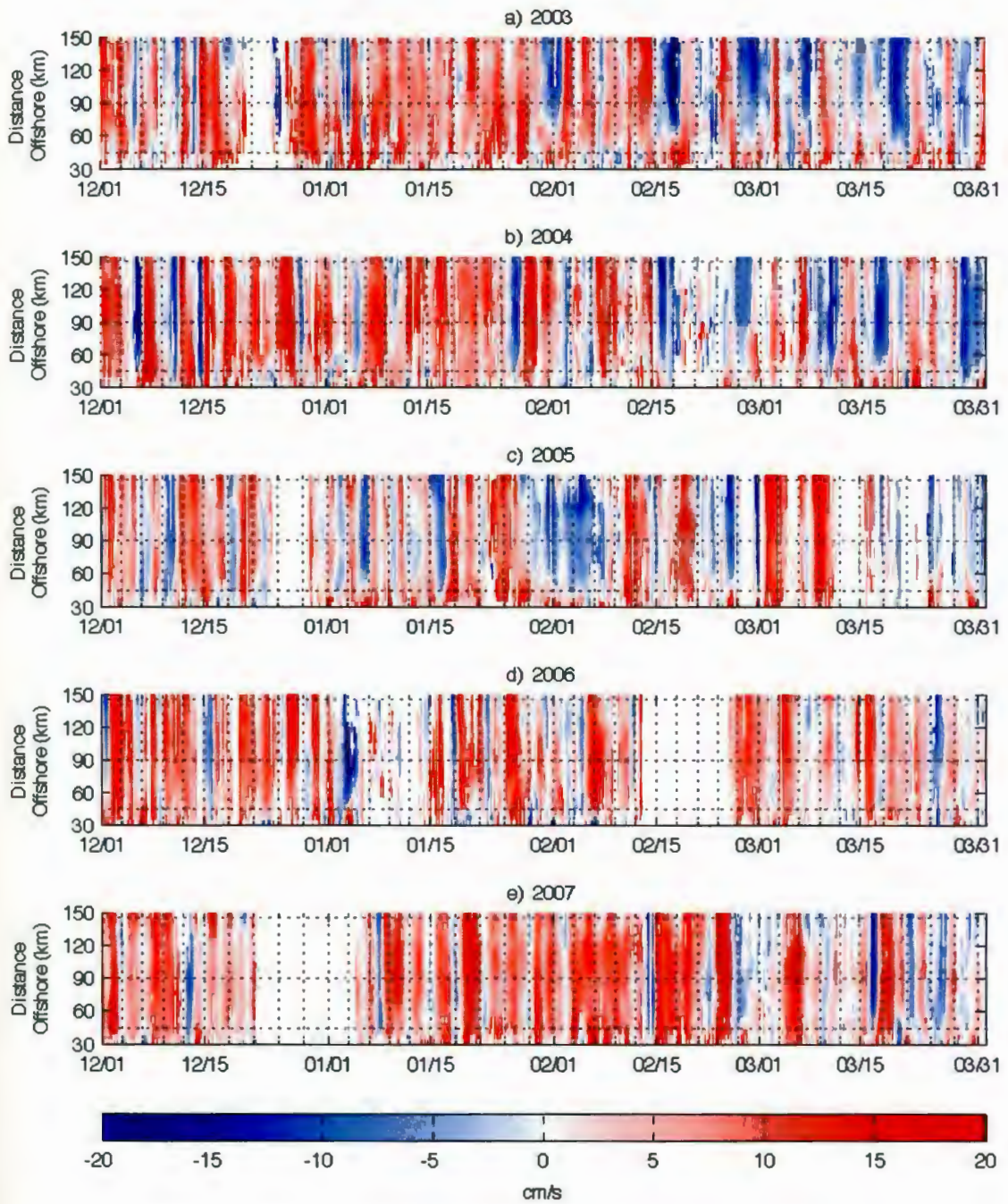


Figure 23. Temporal Variability of Cross-shelf Velocity along Line B: Winters (December-March) a) 2003 b) 2004 c) 2005 d) 2006 e) 2007

Along-shelf Velocity

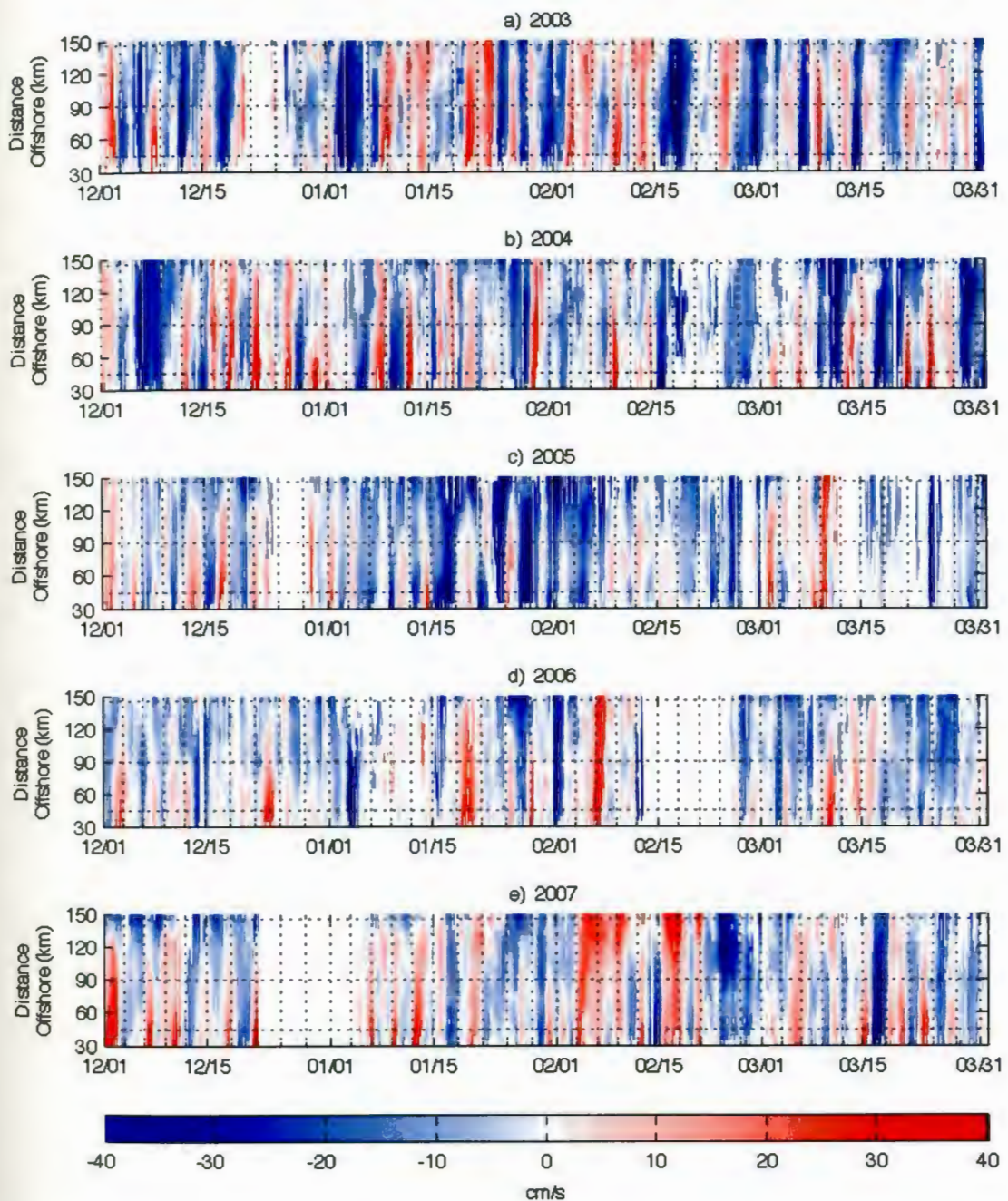


Figure 24. Temporal Variability of Along-shelf Velocity along Line B: Winters (December-March) a) 2003 b) 2004 c) 2005 d) 2006 e) 2007

Mean Current Components : Line B

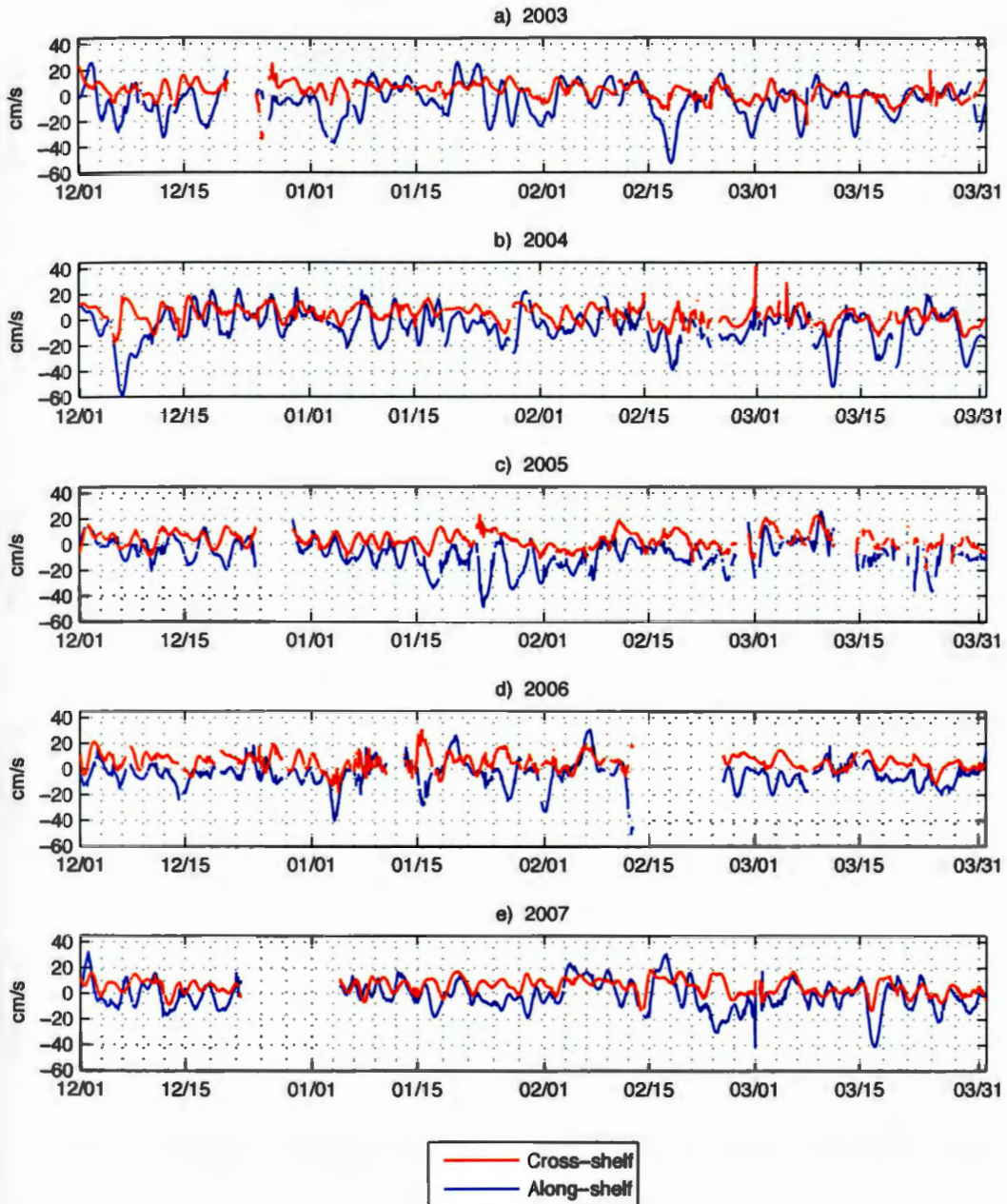


Figure 25. Temporal Variability of Mean Current Components along Line B: Winters (December-March) Cross-shelf Velocity (red) and Along-shelf Velocity (blue) a) 2003 b) 2004 c) 2005 d) 2006 e) 2007

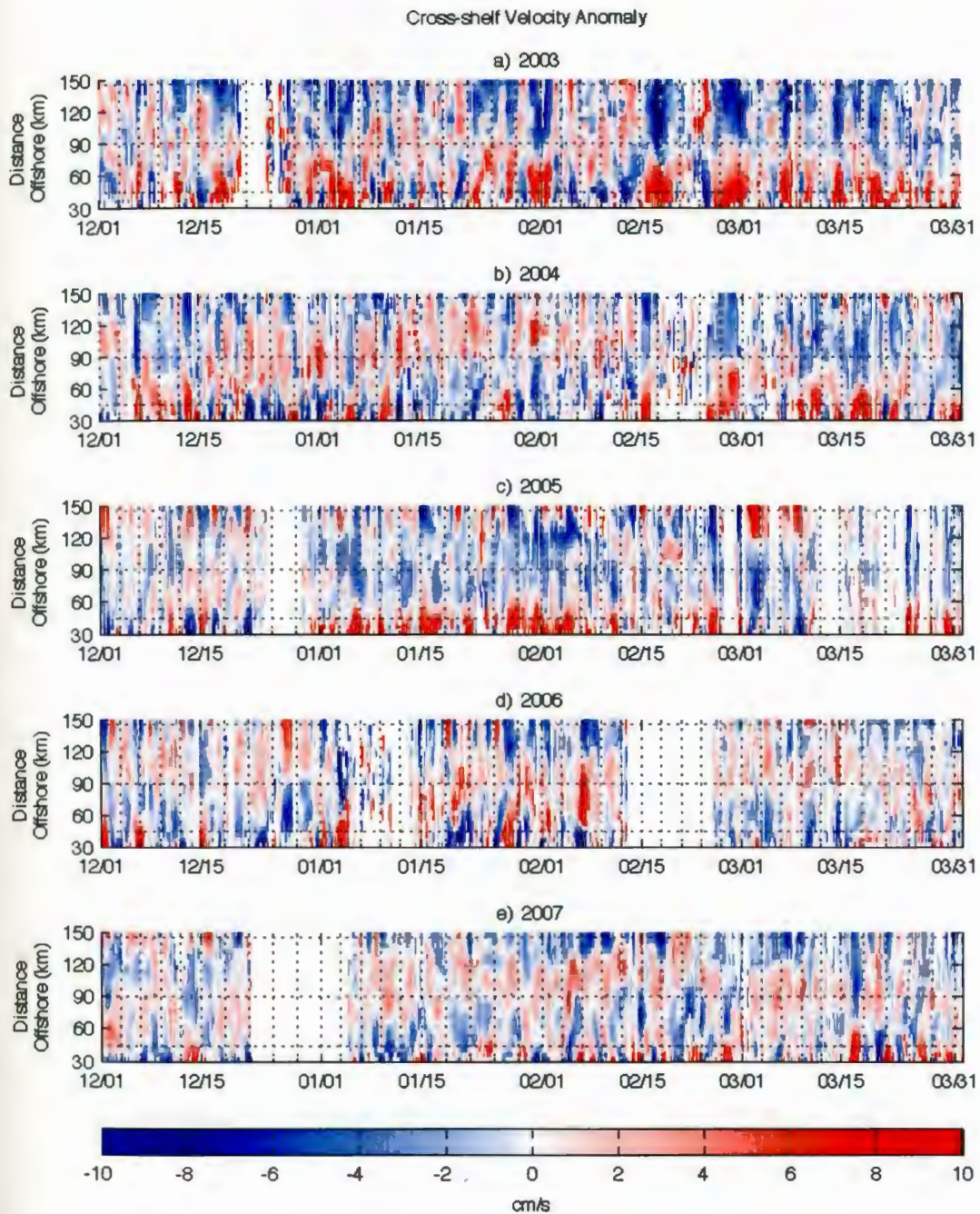


Figure 26. Temporal Variability of Line B Cross-shelf Velocity Anomaly: Winters (December-March)
a) 2003 b) 2004 c) 2005 d) 2006 e) 2007

Along-shelf Velocity Anomaly

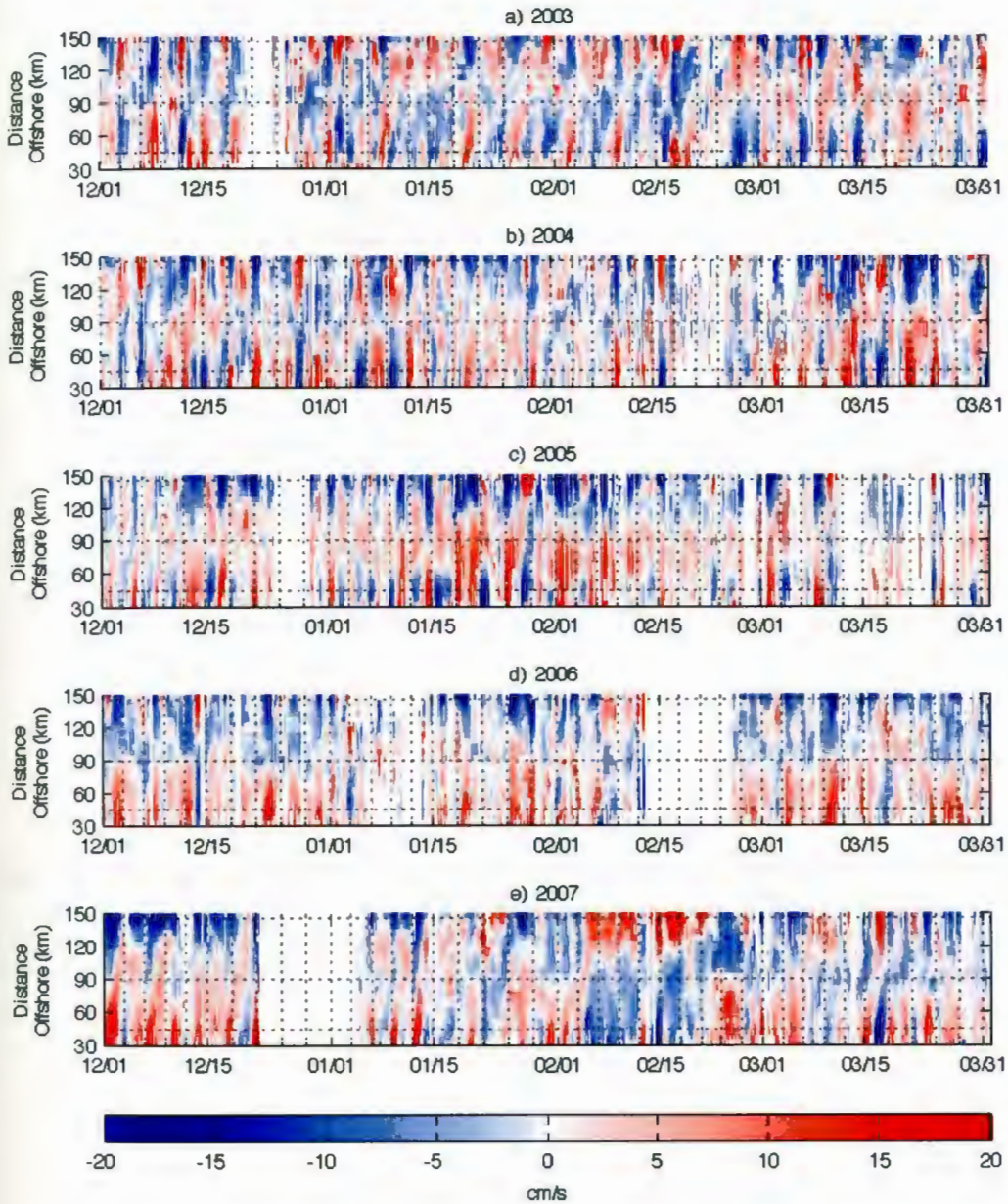


Figure 27. Temporal Variability of Line B Along-shelf Velocity Anomaly: Winters (December-March) a) 2003 b) 2004 c) 2005 d) 2006 e) 2007

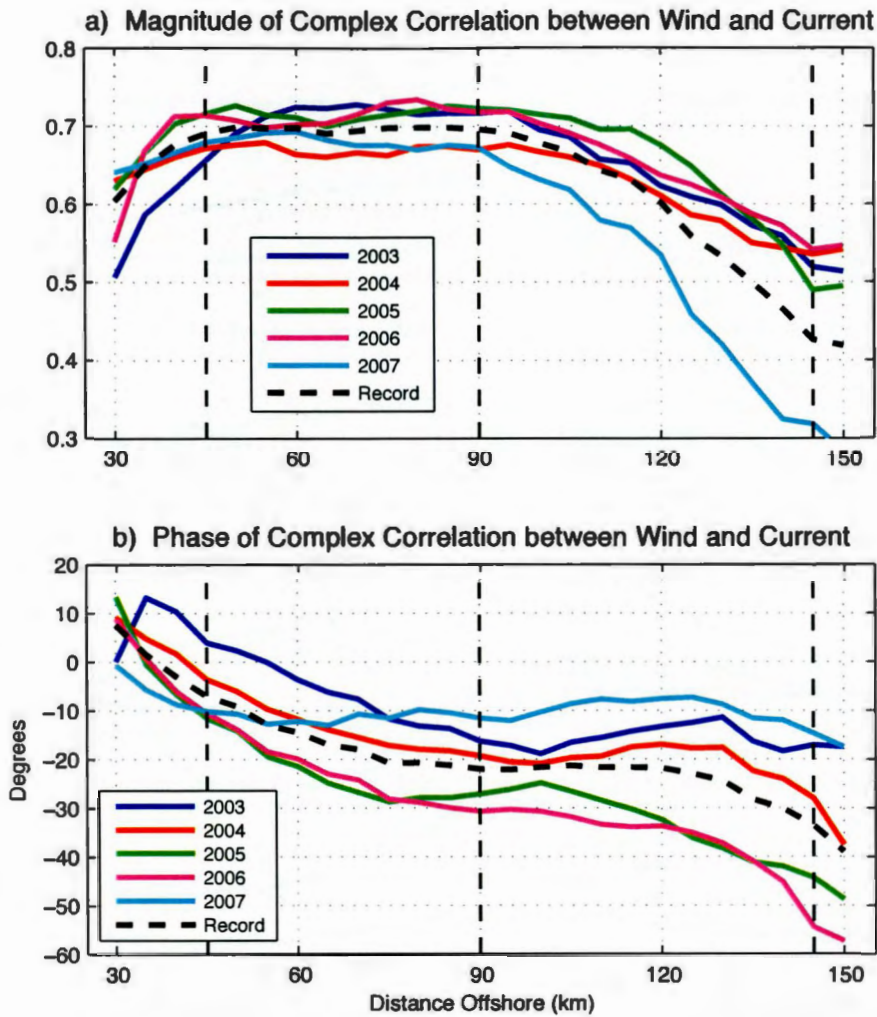


Figure 28. **Correlation between Wind and Current as a function of Offshore Distance:** For each year the a) phase ($^{\circ}$) and b) magnitude between the wind and current were calculated via complex correlation. A negative phase angle indicates the current is to the right (clockwise) of the wind. The vertical, dashed, black lines denote the approximate location of the 30 m, 50 m and 200 m isobaths.

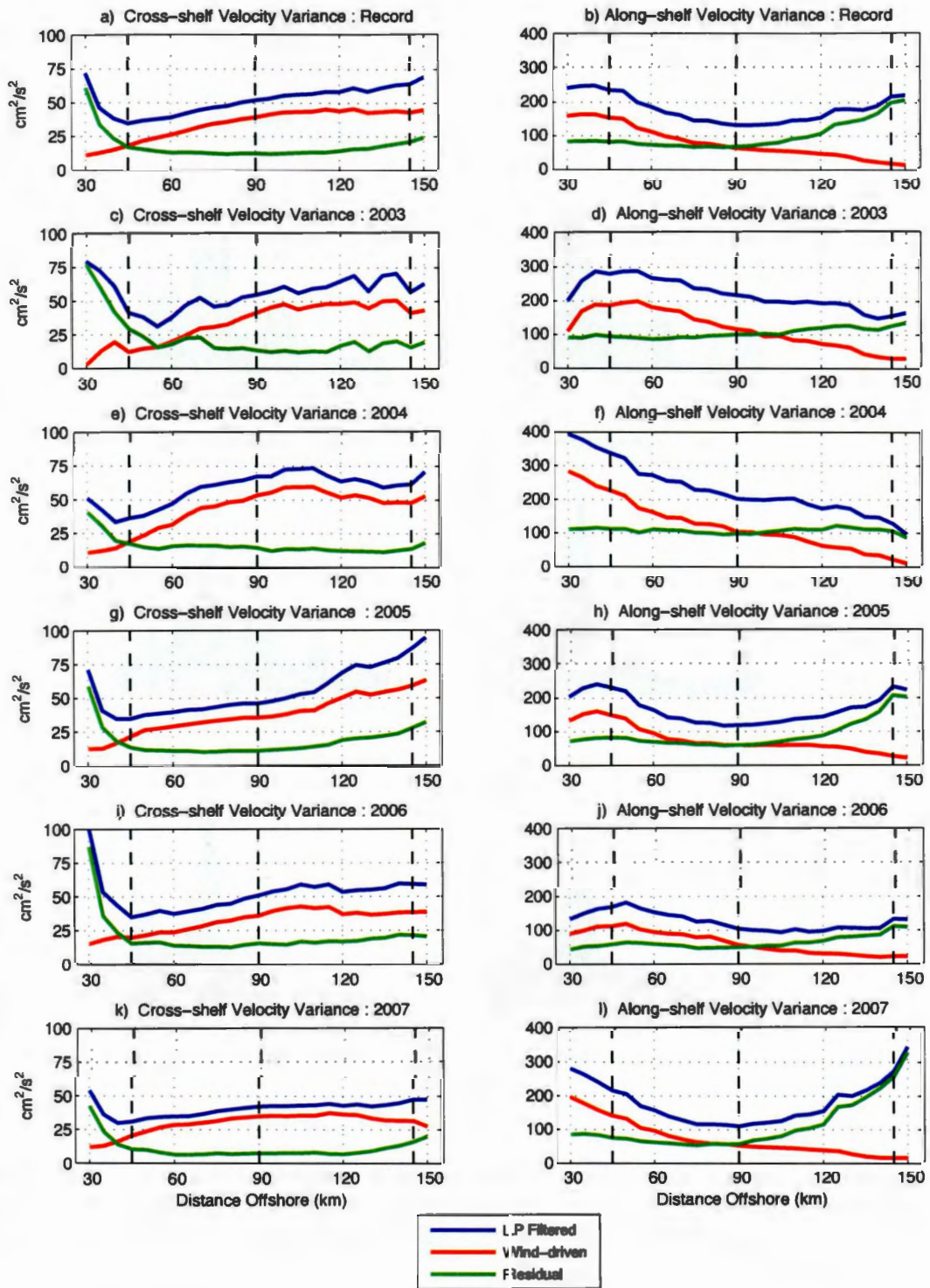


Figure 29. Transient, Wind-driven, and Residual Velocity Variance with Line B Distance Offshore: Winters (December-March) 2003-2007 and Five-year Record Mean a),c),e),g) and i) Cross-shelf Velocity Variance b),d),f),h), and j) Along-shelf Velocity Variance

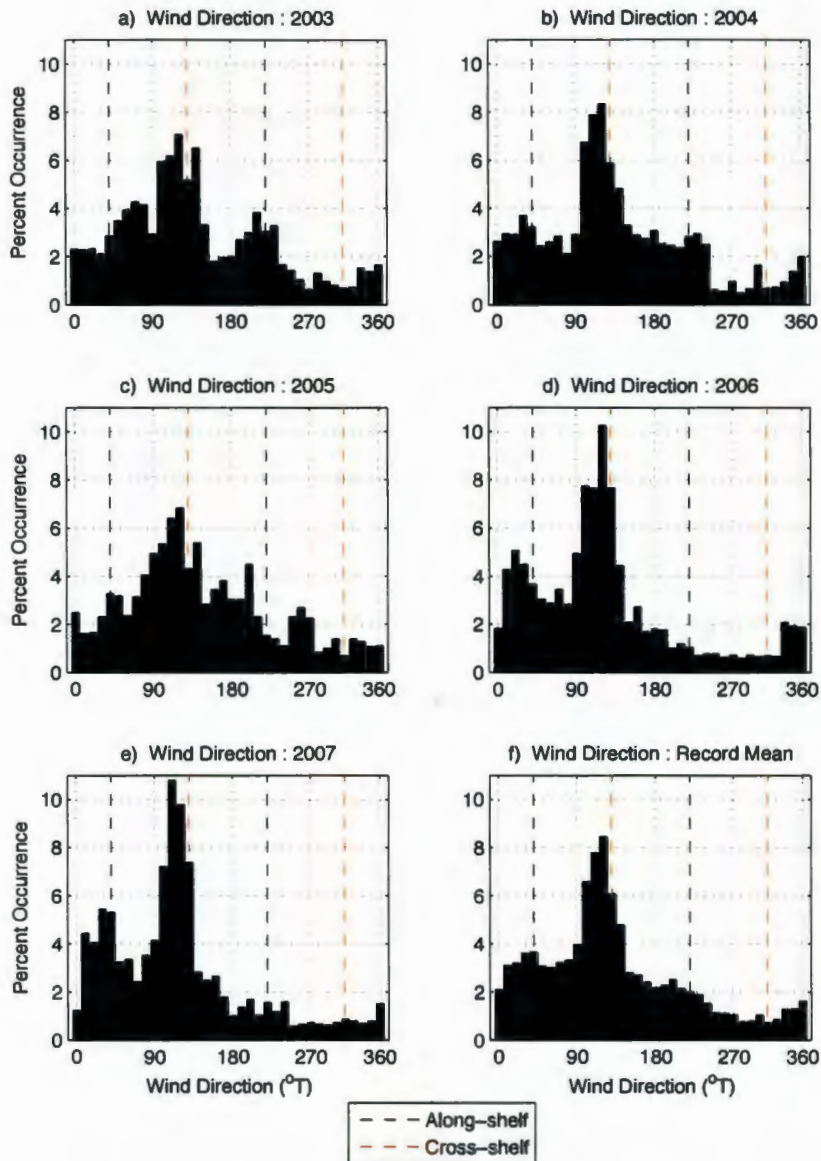


Figure 30. Annual Variation of Wind Direction Distribution: Towards which the wind is blowing in °T. a) 2003 b) 2004 c) 2005 d) 2006 e) 2007 f) Record Mean. The vertical, dashed, black lines denote the along-shelf direction, the vertical dashed, red lines denote the cross-shelf directions

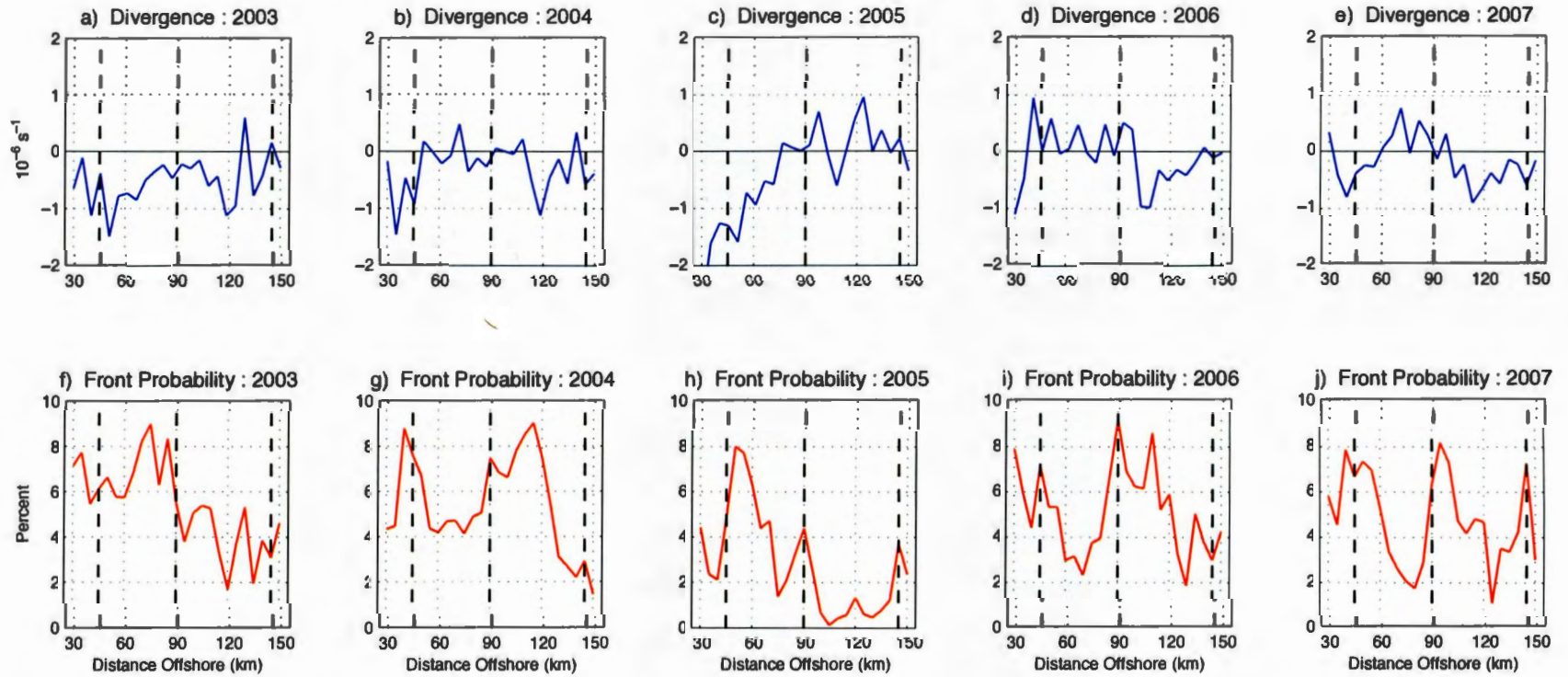


Figure 31. Divergence and Front Probability as a function of Distance Offshore: Winters (December-March) 2003-2007 a),c),e),g), and i) Box 30 b),d),f),h), and j) Box 50.

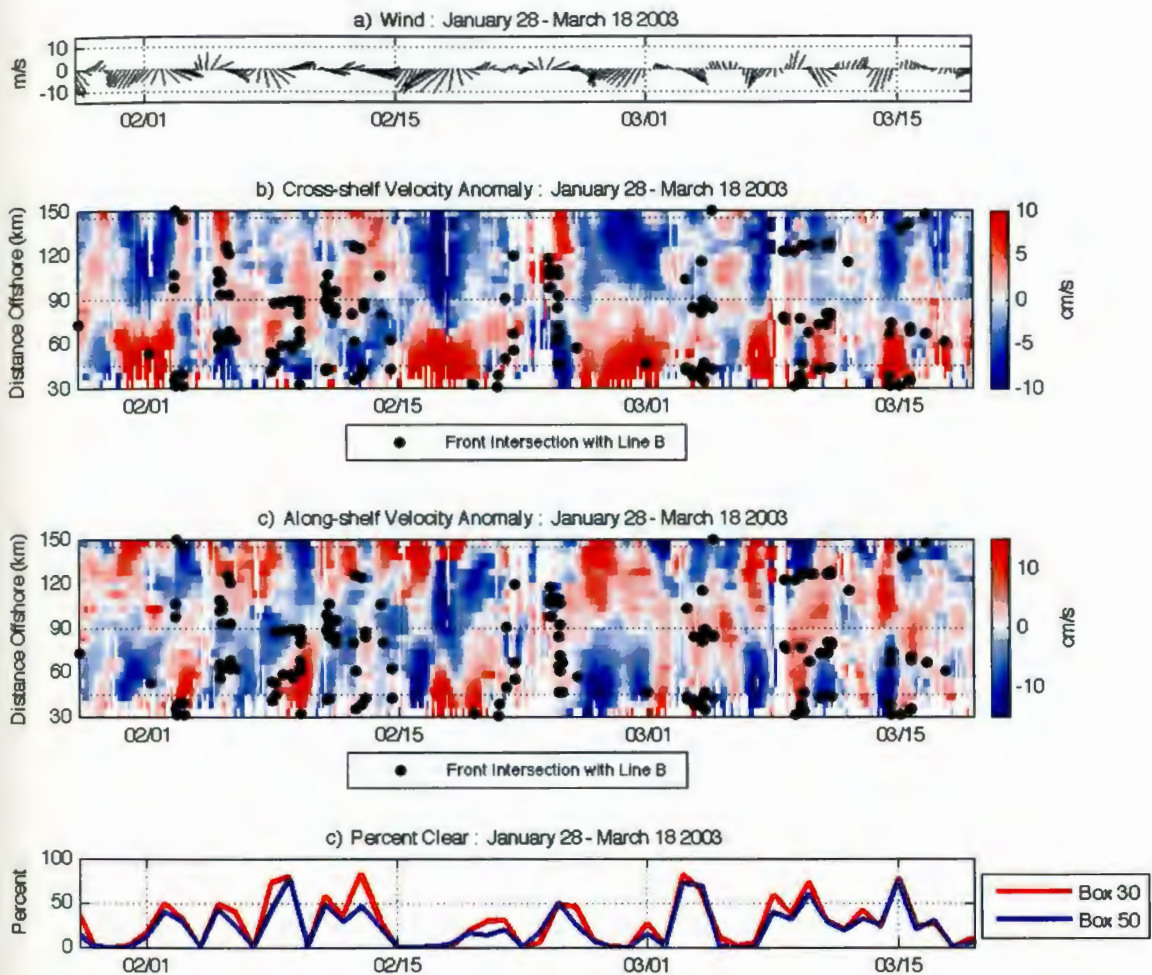


Figure 32. Composite Analysis of January 28 - March 18 2003: a) Wind b) Line B : Cross-shelf Velocity Anomaly and Intersecting Fronts c) Line B : Along-shelf Velocity Anomaly and Intersecting Fronts d) Percent Clear in Box 30 and Box 50. The thin, dotted black lines at 45 km, 90 km and 145 km denote the 30 m, 50 m and 200 m isobaths.

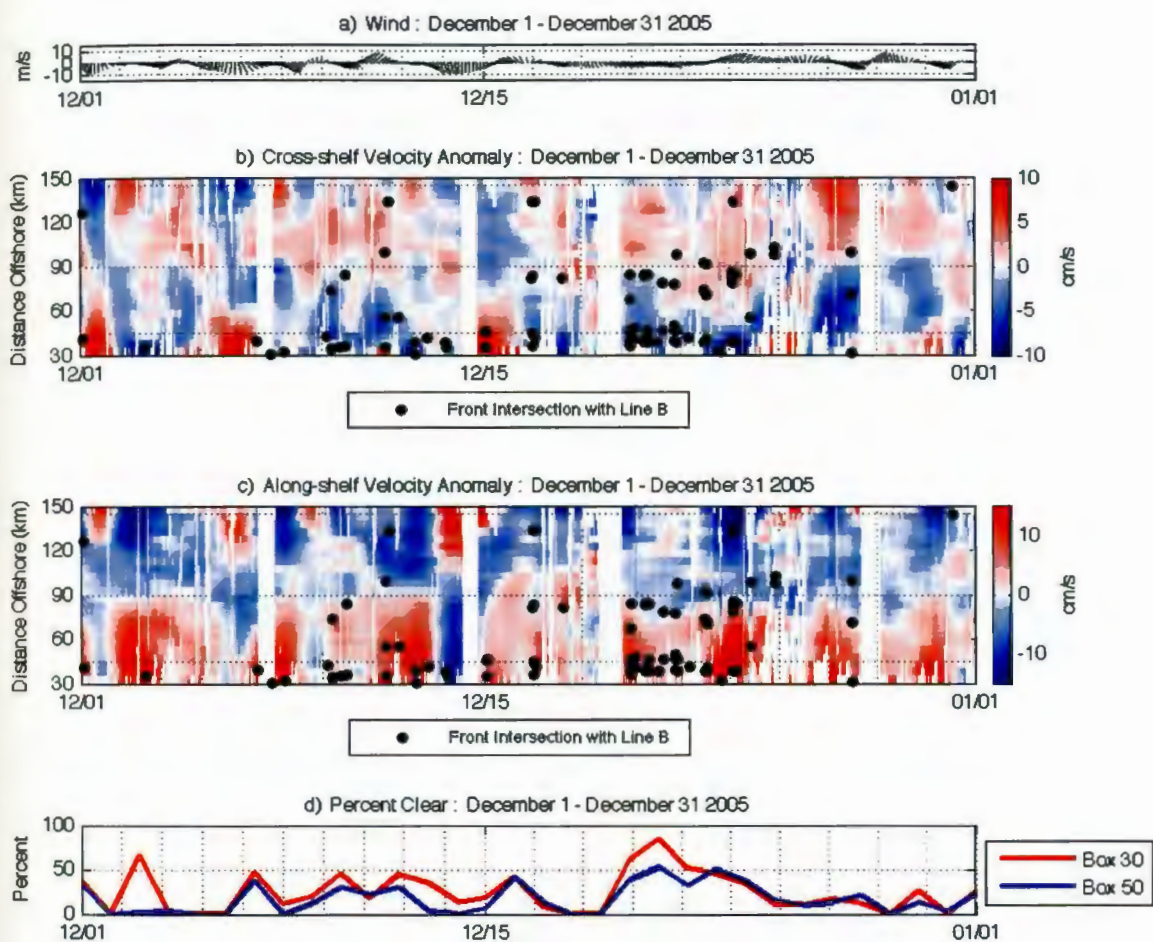


Figure 33. **Composite Analysis of December 1 - December 31 2005:** a) Wind b) Line B : Cross-shelf Velocity Anomaly and Intersecting Fronts c) Line B : Along-shelf Velocity Anomaly and Intersecting Fronts d) Percent Clear in Box 30 and Box 50. The thin, dotted black lines at 45 km, 90 km and 145 km denote the 30 m, 50 m and 200 m isobaths.

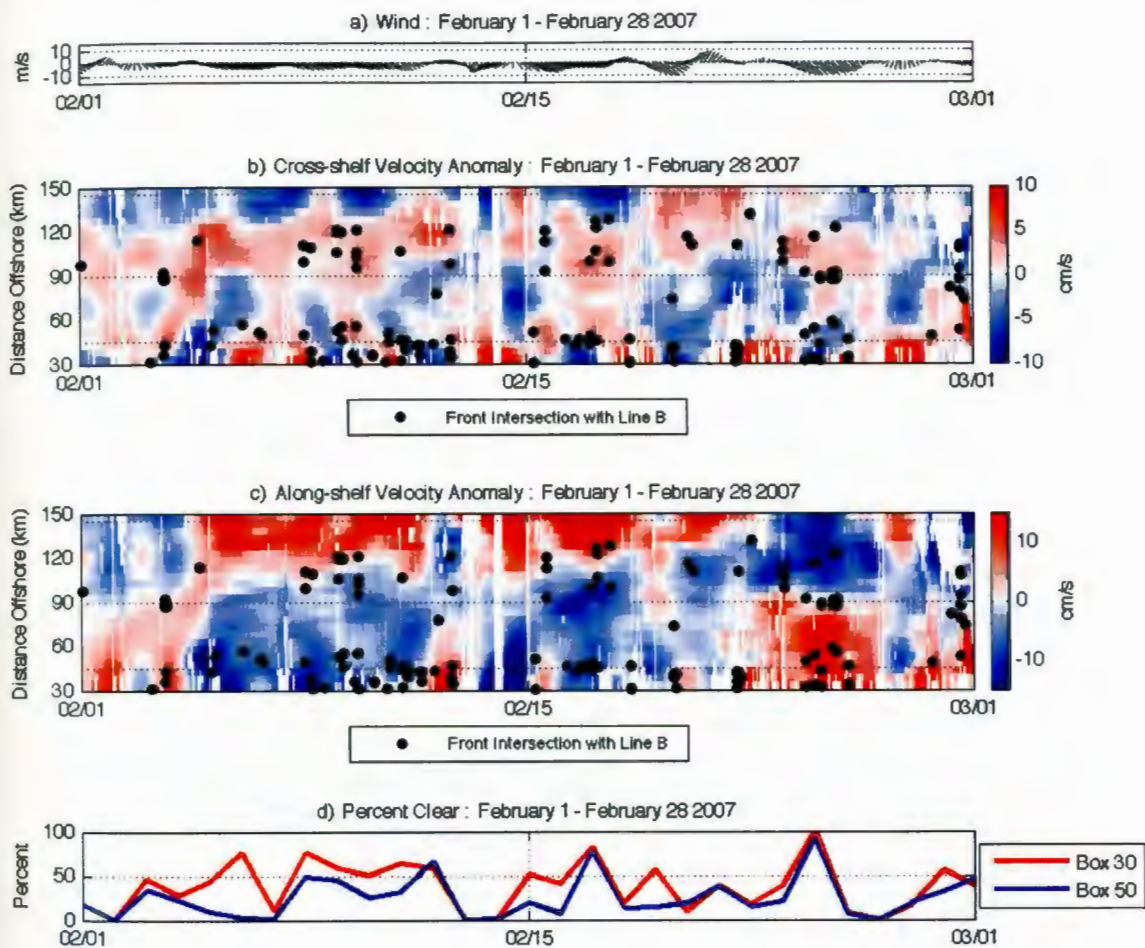


Figure 34. **Composite Analysis of February 1 - February 28 2007:** a) Wind b) Line B : Cross-shelf Velocity Anomaly and Intersecting Fronts c) Line B : Along-shelf Velocity Anomaly and Intersecting Fronts d) Percent Clear in Box 30 and Box 50. The thin, dotted black lines at 45 km, 90 km and 145 km denote the 30 m, 50 m and 200 m isobaths.

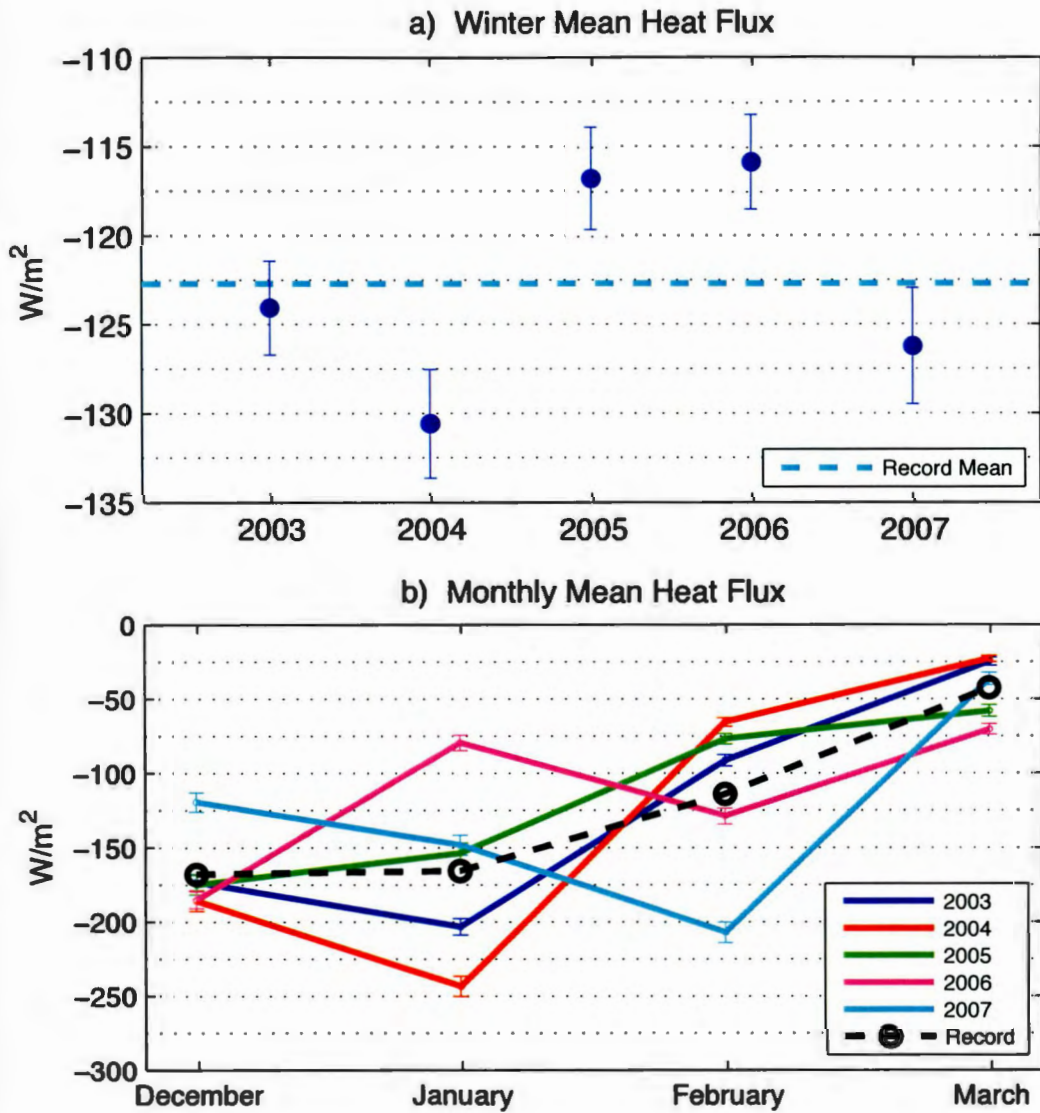


Figure 35. Winter and Monthly Variation of Heat Flux: Equals the sum of Sensible and Latent Heat
 a) Annual Variation of Heat Flux b) Monthly Variation of Heat Flux.

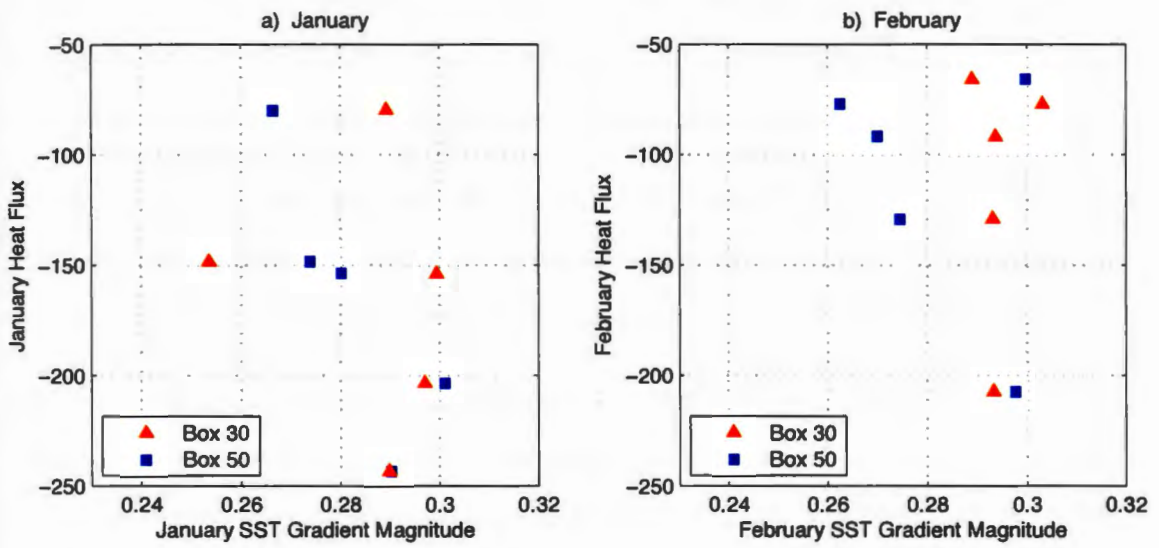


Figure 36. Heat Flux versus SST Gradient Magnitude: a) January b) February.

Bibliography

- Beardsley, R. C., W. C. Boicourt, and D. V. Hansen (1976), Physical oceanography of the Middle Atlantic Bight, in *Limnology and Oceanography Special Symposium*, vol. 2, pp. 20–34.
- Blanton, J. O. (1986), Coastal frontal zones as barriers to offshore fluxes of contaminants, *Rapports et Procès-Verbaux des Réunions, Conseil International pour l'Exploration de la Mer*, 186, 18–30.
- Breaker, L. C., T. C. Mavor, and W. W. Broenkow (2005), *Mapping and monitoring large-scale ocean fronts off the California Coast using imagery from GOES-10 geostationary satellite*, Available at http://repositories.cdlib.org/csgc/rcr/Coastal05_02, (accessed on 05 June 2008).
- Brunetti, N. E., B. Elena, G. R. Rossi, M. L. Ivanovic, A. Aubone, R. Guerro, and H. Benavides (1998), Summer distribution, abundance and population structure of *illex argentinus* on the argentine shelf in relation to environmental features, *S. Afr. Mar. Sci.*, 20, 175–178.
- Castelao, R. M., S. M. Glenn, O. Schofield, R. J. Chant, J. Wilkin, and J. T. Kohut (2008), Seasonal evolution of hydrographic fields in the central Middle Atlantic Bight from glider observations, *Geophysical Research Letters*, 35, L03,617, doi:10.1029/2007GL032,335.
- Cayula, J.-F., and P. Cornillon (1992), Edge-detection algorithm for SST images, *Journal of Atmospheric and Oceanic Technology*, 9, 67–80.
- Cayula, J.-F., and P. Cornillon (1995), Multi-image edge detection for SST images, *Journal of Atmospheric and Oceanic Technology*, 12, 821–829.
- Chang, Y., T. Shimada, M.-A. Lee, H.-J. Lu, F. Sakaida, and H. Kawamura (2006), Wintertime sea surface temperature fronts in the taiwan strait, *Geophysical Research Letters*, 33, L23,603, doi:10.1029/2006GL027,415.
- Csanady, G. T. (1978), Wind effects on surface to bottom fronts, *Journal of Geophysical Research*, 83, 4633–4640.

- Dzwonkowski, B., J. T. Kohut, and X.-H. Yan (2008a), Seasonal differences in wind-driven cross-shelf forcing and response relationships in the mid-shelf surface layer of the central Mid-Atlantic Bight, *manuscript in Journal of Geophysical Research review*.
- Dzwonkowski, B., B. L. Lipphardt, X.-H. Yan, J. T. Kohut, and R. W. Garvine (2008b), Observations of surface layer, sub-inertial, across-shelf flows on the mid-shelf of the central Mid-Atlantic Bight, *manuscript in Journal of Geophysical Research review*.
- Fairall, C. W., E. F. Bradley, D. P. Rogers, J. B. Edson, and G. S. Young (1996), Bulk parameterization of air-sea fluxes for TOGA COARE, *Journal of Geophysical Research*, *101*, 3747–3764.
- Federov, K. N. (1986), *The Physical Nature and Structure of Oceanic Fronts*, Springer-Verlag, New York.
- Fratantoni, P. S., R. S. Pickart, D. J. Torres, and A. Scott (2001), Mean structure and dynamics of the shelfbreak jet in the Middle Atlantic Bight during fall and winter, *Journal of Physical Oceanography*, *31*, 2135–2156.
- Gong, D., R. J. Chant, S. M. Glenn, J. T. Kohut, and J. Wilkin (2006), *NJ Turnpike - Transport Pathways on the NY Bight*, Available at www.marine.rutgers.edu/mrs/coolresult/2005/donglai_OS2006talk.ppt, (accessed 16 August 2007).
- Hickox, R., I. Belkin, P. C. Cornillon, and Z. Shan (2000), Climatology and seasonal variability of ocean fronts in the East China, Yellow and Bohai Seas from satellite SST data, *Geophysical Research Letters*, *27*(18), 2945–2948.
- Hill, A., and J. Simpson (1989), On the interaction of thermal and haline fronts: The Islay Front revisited, *Estuarine, Coastal and Shelf Science*, *28*(495-505).
- Hoskins, B. J. (1982), The mathematical theory of frontogenesis, *Annual Review of Fluid Mechanics*, *14*, 131–151.

- Huh, O. K., W. J. Wiseman, and L. J. R. Jr. (1978), Winter cycle of sea surface thermal patterns, northeastern Gulf of Mexico, *Journal of Geophysical Research*, 83, 4523–4529.
- Kohut, J. T., S. M. Glenn, and R. J. Chant (2004), Seasonal current variability on the New Jersey inner shelf, *Journal of Geophysical Research*, 109, C07S07, doi:10.1029/2003JC001,963.
- Lipa, B., and D. Barrick (1986), Least-squares methods for the extraction of surface currents from CODAR crossed-loop data: application at ARSLOE, *IEEE Journal of Ocean Engineering*, OE-8, 226–253.
- Mooers, C. N. K., J. Fernandez-Partagas, and J. F. Price (1976), Meteorological forcing fields of the New York Bight (first year's progress report), *Technical Report TR76-8*, Rosentiel School of Marine and Atmospheric Science, University of Miami, Miami, FL.
- Narayanan, C., and R. W. Garvine (2002), Large scale buoyancy driven circulation on the continental shelf, *Dynamics of Atmospheres and Oceans*, 36, 125–152.
- Oey, L.-Y. (1986), The formation and maintenance of density fronts on the U.S. southeastern continental shelf during winter, *Journal of Physical Oceanography*, 16, 1121–1135.
- Ou, H. W., R. C. Beardsley, D. Mayer, W. C. Boicourt, and B. Butman (1981), An analysis of subtidal fluctuations in the Middle Atlantic Bight, *Journal of Physical Oceanography*, 11, 1383–1392.
- Ou, H.-W., C.-M. Dong, and D. Chen (2003), Tidal Diffusivity: A mechanism for frontogenesis, *Journal of Physical Oceanography*, 33, 840–847.
- Press, W. H., S. A. Teukolsky, W. T. Vetterling, and B. P. Flannery (1992), *Numerical Recipes in FORTRAN: The art of scientific computing*, 2nd ed., Cambridge University Press.
- Robinson, I. S. (1985), *Satellite Oceanography: An Introduction for Oceanographers and Remote-Sensing Scientists*, 244-246, Ellis Horwood, Chichester, England.
- Romero, S. I., A. R. Piola, M. Charo, and C. A. E. Garcia (2006), Chlorophyll a variability

off Patagonia based on SeaWiFS data, *Journal of Geophysical Research*, 111(C5), C05,021, 10.1029/2005JC003,244.

Saunders, P. M. (1977), Wind stress on the ocean over the eastern continental shelf of North America, *Journal of Physical Oceanography*, 7, 555–566.

Ullman, D. S., and P. C. Cornillon (1999), Satellite derived sea surface temperature fronts on the continental shelf off the northeast U.S. coast, *Journal of Geophysical Research*, 104(C10), 459–478.

Ullman, D. S., and P. C. Cornillon (2001), Continental shelf surface thermal fronts in winter off the northeast U.S. coast, *Continental Shelf Research*, 21, 1139–1156.

Whitney, M. M., and R. W. Garvine (2005), Wind influence on a coastal buoyant outflow, *Journal of Geophysical Research*, 110, C03,014, doi:10.1029/2003JC002,261.

Yankovsky, A. E., and D. C. Chapman (1997), A simple theory for the fate of buoyant coastal discharges, *Journal of Physical Oceanography*, 27, 1386–1401.